Hydrodynamic modeling in support of the development of the Northeast Corridor Reserve Management Plan

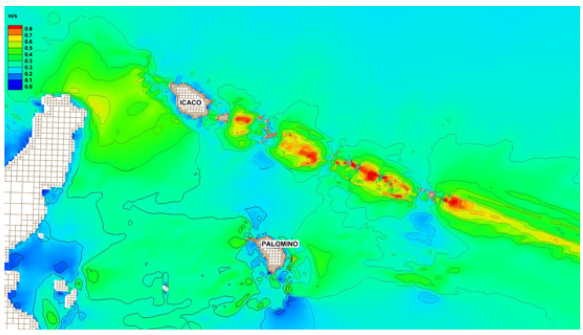

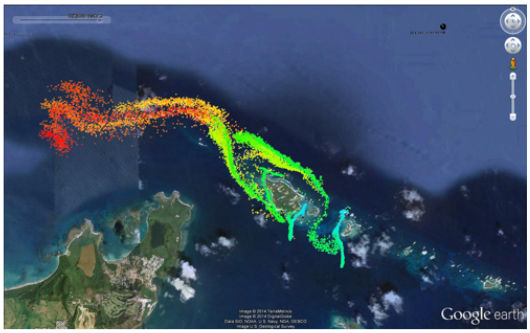

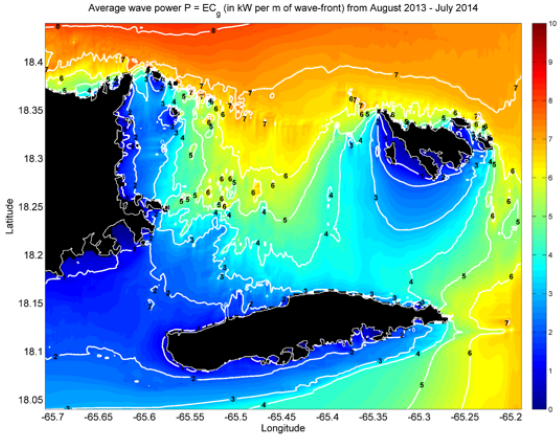

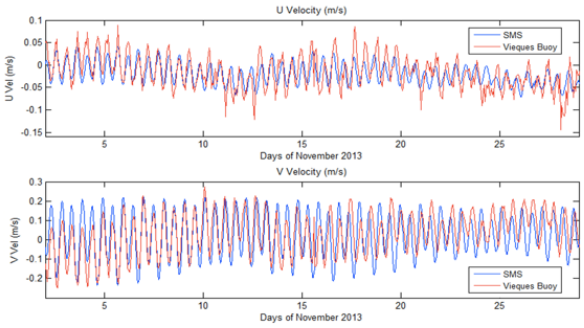

Progress report submitted to:

NOAA Coral Reef Conservation Program

Prepared by:

Miguel Canals, Ph.D.

UPRM Center for Applied Ocean Science and Engineering

Contents

List of Figures

Chapter 1

Introduction

The development of an appropriate management plan for the marine section of the Northeast Corridor Reserve (NECR) requires an understanding of the hydrodynamic forcing of the area and how this forcing affects the spatial distribution of critical biological communities, especially coral reefs. It is well known that the hydrodynamics of coral reefs are affected by physical processes at multiple space and time scales which can drive coral reef zonation (Acevedo et al., 1989). Issues such as the hydrodynamic connectivity between the different regions within the NECR as well as the distribution of wave energy within the region can impact important decisions regarding marine spatial planning in the reserve. In addition, knowledge of the prevailing circulation patterns in the region can help coastal managers determine which areas must be given special attention.

The present study was funded by the NOAA Coral Reef Conservation Program as part of a broader project to gather biological, benthic, geospatial, socio-economical and hydrodynamic data in preparation for the drafting of a management plan for the NECR. The present progress report is divided into three chapters as follows:

- **Chapter 2 - Wave modeling of the NECR**: This chapter provides an overview of the main results from high-resolution numerical wave modeling for the region, including maps of the annual average wave power. In addition, as part of the present study, an operational wave model for the NECR has been developed and is available `http://www.caricoos.org/drupal/swan_multigrid/NECR`.

- **Chapter 3 - Circulation modeling of the NECR**: This chapter provides a description of the implementation of a high-resolution circulation model of the NECR, including the validation of the model using buoy data. Maps of the spatial distribution of the average and maximum current velocities within the NECR are also provided.

- **Chapter 4 - Preliminary particle transport modeling (PTM) in the NECR**: This chapter provides some preliminary results from particle tracking modeling within the NECR.

The role that the complex spatial structure of the wave power and current velocity fields described in Chapters 3 and 4 play in the distribution of endangered coral species such as elkhorn coral within the NECR remains to be determined. These datasets have been shared with the NOAA Biogeography Group for inclusion into their online NECR spatial database. It is expected that this data will be useful for marine spatial planning efforts within the NECR. The PTM simulations presented herein are only two preliminary simulations with arbitrary durations and source locations. Future simulations should include input from coastal managers working within the NECR in order to use the simulations to address larval connectivity or sediment loading issues within the NECR.

Chapter 2

Wave modeling of the NECR

2.1 SWAN wave model

The CariCOOS Nearshore wave model is an operational model forced by spectral data from the NOAA WaveWatch III model and with surface winds from the National Weather Service National Digital Forecast Database. Details of the model setup and validation may be found in Anselmi et al. (2012), Canals et al. (2012) and Canals (2014). The model was modified to include high-resolution nested grids in order to resolve wave transformation processes within the NECR, taking into account the complex bathymetry of the region. The model is currently operational, including the NECR grids, at `http://www.caricoos.org/drupal/swan_multigrid`.

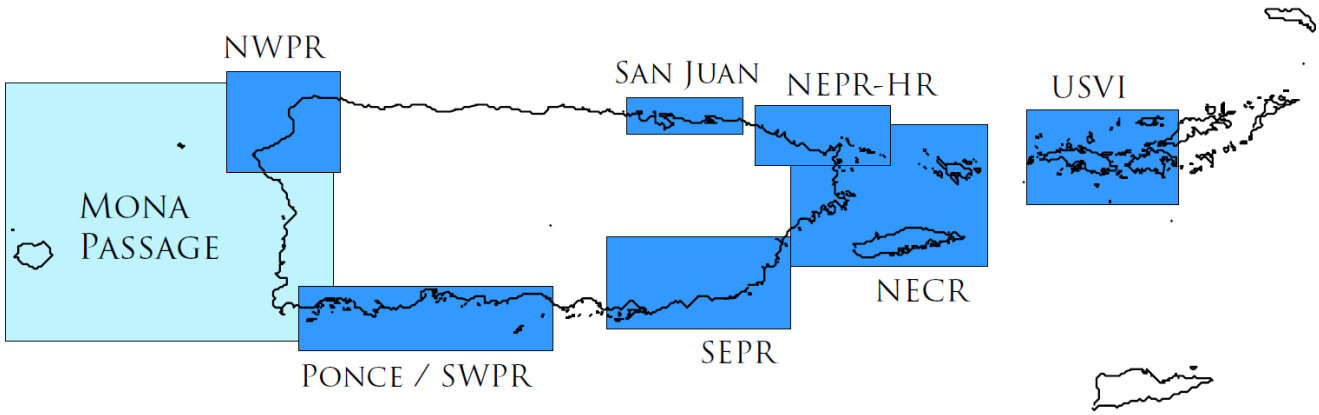

Figure 2.1: Grids of the CariCOOS Nearshore Wave Model.

In order to understand the spatial distribution of wave energy within the NECR, two high-resolution nested grids were developed specifically for the present study, as shown in Figure 2.1:

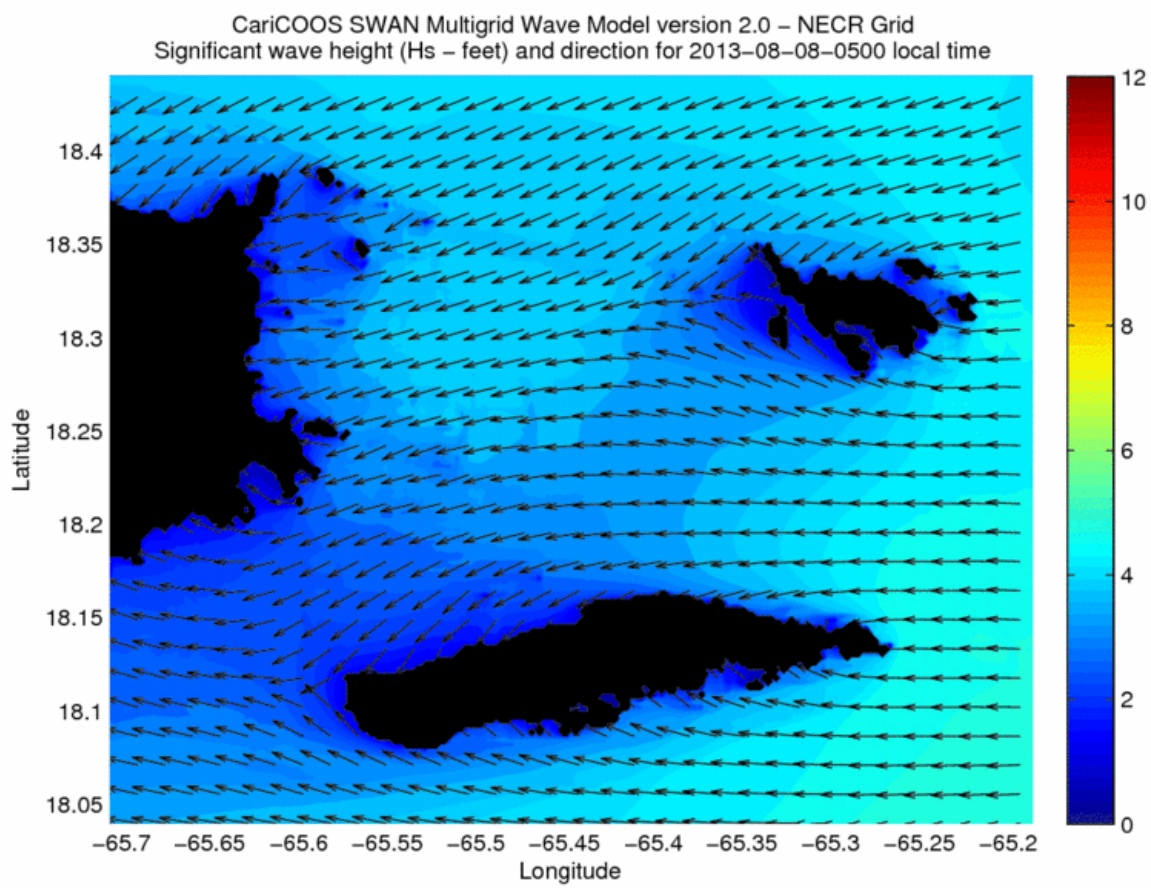

Figure 2.2: Sample output of significant wave height (colors) and wave direction (arrows) for the NECR grid, which focuses on the Fajardo / La Cordillera / Culebra areas of the NECR.

NECR The NECR grid was developed in August 2013 and includes most of the NECR, as well as the islands of Vieques and Culebra. The spatial resolution is 240 meters.

NEPR The NEPR grid was finalized in February 2014 and includes the coral reefs of Rio Grande, Luquillo and Fajardo, including Las Cabezas de San Juan. The spatial resolution is 120 meters.

The bathymetry for these grids was obtained from the $1/3$ arc-sec NGDC Digital Evevation Model for Puerto Rico Taylor et al. (2006). Sample output for each of these grids is shown in Figures 2.2 and 2.3.

2.2 Wave statistics

At the time of the writing of this report (July 2014), the NECR has been running for 1 year and the NEPR for 6 months. The wave data from this time period has been used to compute the spatial distribution of

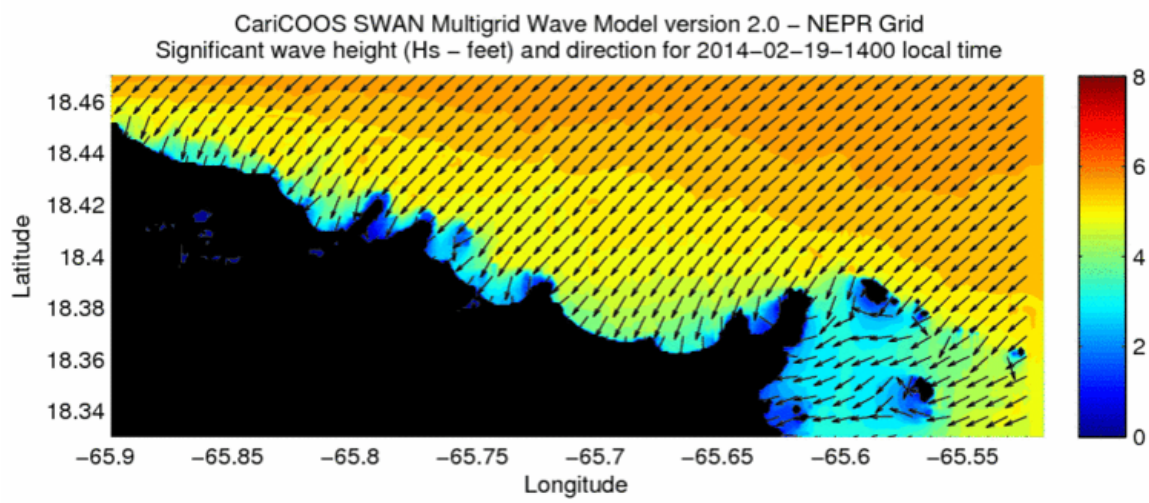

Figure 2.3: Sample output of significant wave height (colors) and wave direction (arrows) for the NEPR grid, which focuses on the Rio Grande, Luquillo and Fajardo areas of the NECR, including Las Cabezas de San Juan.

the time averaged significant wave height for each grid for the corresponding time period. The results are shown in Figures 2.4 and 2.5 for the NECR and NEPR grids, respectively. Note the drastic reduction of the average wave height shoreward of the coral reef areas and the role of the La Cordillera reefs in the dissipation of wave energy.

The actual wave power which impacts the region depends not only on the wave height but also on the period of the incoming wave trains as well as on the local water depth. The wave power (in kW) per meter of wave crest is given by:

$$P = EC_g \tag{2.1}$$

where E is the wave energy density per unit area and C_g is the wave group speed. The wave energy density per unit area E is given by:

$$E = \frac{1}{16}\rho g H^2 \tag{2.2}$$

where H is the wave height, ρ the seawater density, and g the gravitational constant. The wave group speed, C_g, is given by:

$$C_g = \frac{1}{2}\left\{1 + \frac{4\pi d/L}{\sinh(4\pi d/L)}\right\}\frac{L}{T} \tag{2.3}$$

where d is the local water depth and L is the local wavelength, which is obtained by solving the full wave dispersion relation:

$$\omega^2 = gk \tanh kh \tag{2.4}$$

where $\omega = 2\pi/T$ is the wave angular frequency and $k = 2\pi/L$ is the wavenumber. For this study the wavelength as a function of time and space has been obtained by solving the above dispersion relation equation using the Newton-Raphson method in MATLAB.

The wave power per unit meter of wave crest, P, has been averaged over the available time period (August 2013 to July 2014 for the NECR grid, and February 2014 to July 2014 for the NEPR grid) for each grid. The results are shown in Figures 2.6 and 2.7 for the NECR and NEPR grids, respectively. Since these grids are operational within the CariCOOS Nearshore Wave Model and are run twice per day every day, these figures can be revisited later on when more data is available.

The role that the complex spatial structure of the wave energy field plays in the distribution of endangered coral species such as elkhorn coral within the NECR remains to be determined. These datasets have been shared with the NOAA Biogeography Group for inclusion into their online NECR spatial database. It is expected that this data will be useful for marine spatial planning efforts within the NECR.

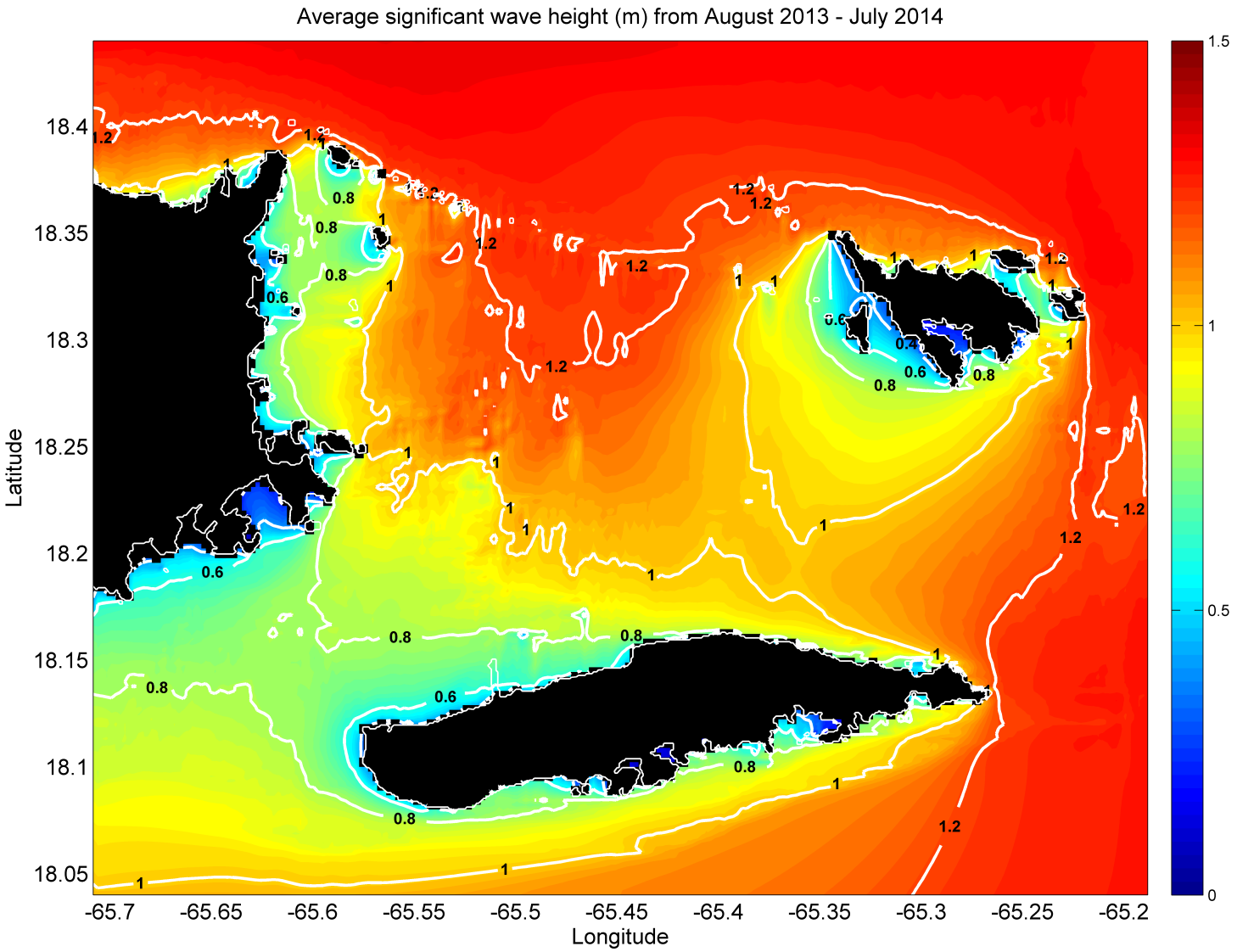

Figure 2.4: Average wave height from August 2013 to July 2014 for the Fajardo / La Cordillera grid of the NECR.

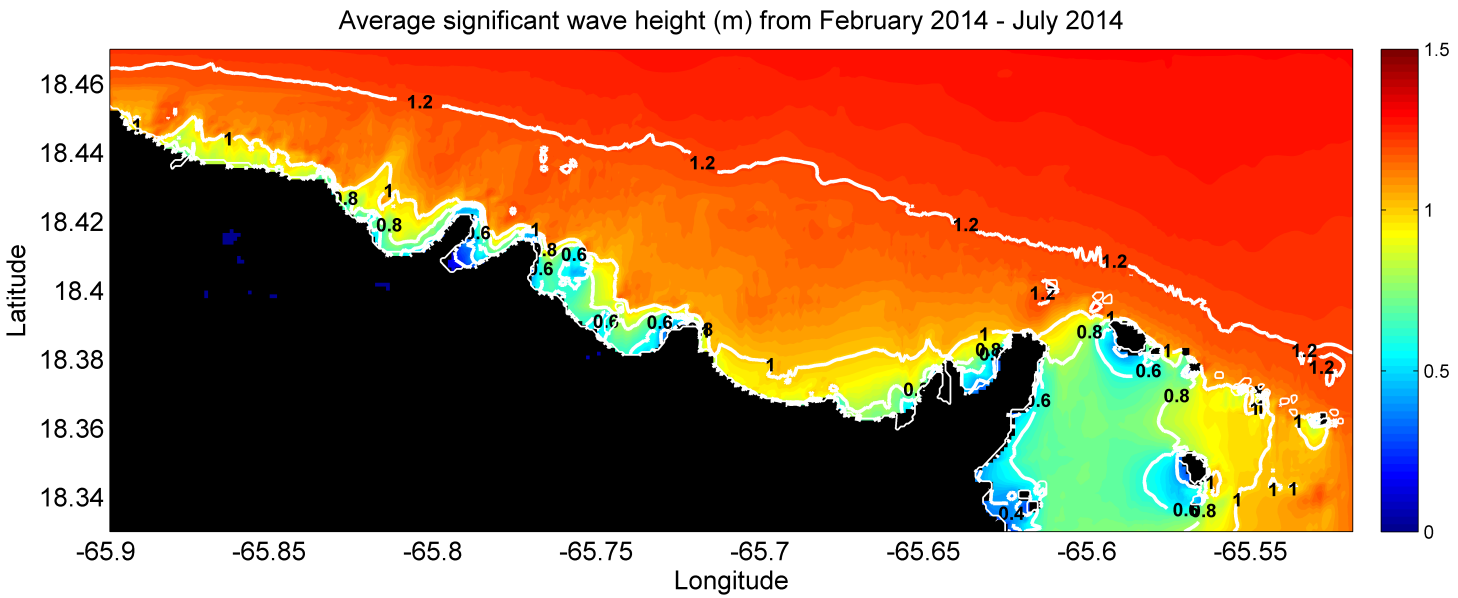

Figure 2.5: Average wave height from February 2014 to July 2014 for the Rio Grande / Luquillo grid of the NECR.

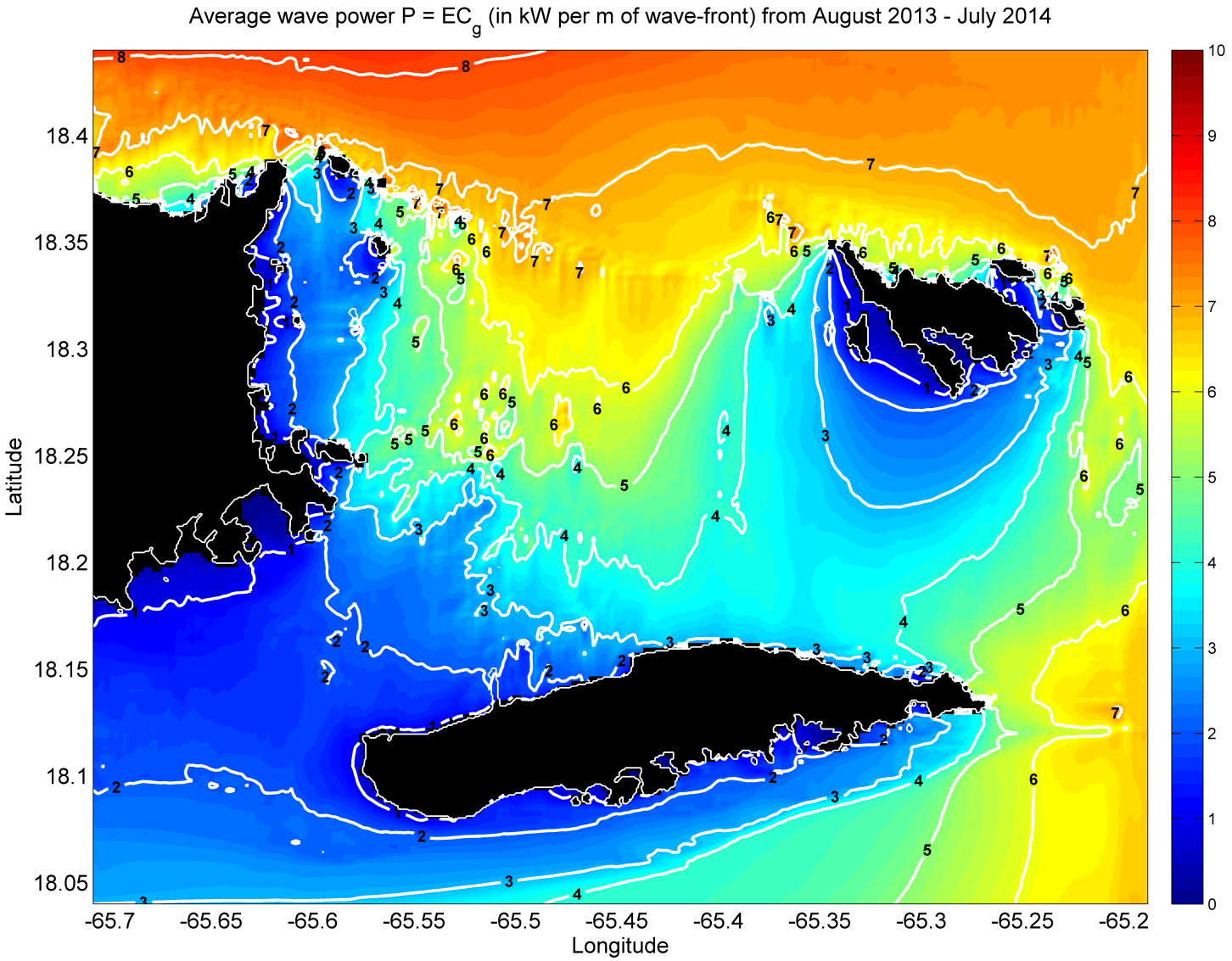

Figure 2.6: Average wave power in kW/m from August 2013 to July 2014 for the Fajardo / La Cordillera grid of the NECR.

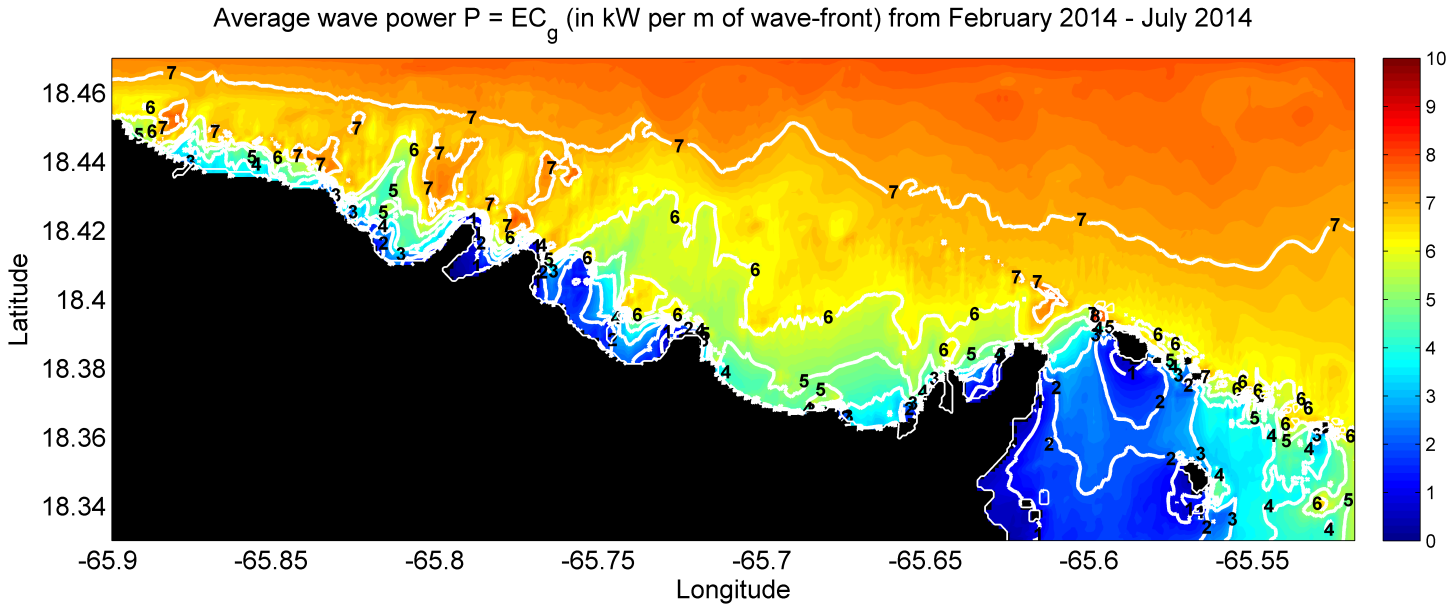

Figure 2.7: Average wave power in kW/m from February 2014 to July 2014 for the Rio Grande / Luquillo grid of the NECR.

Chapter 3

Circulation modeling of the NECR

The main focus of the present study was to develop a coastal circulation model for the NECR in order to develop the capabilities of simulating particle transport and eventually being able to quantify hydrodynamic connectivity within the reserve. The spatial resolution of existing operational models is currently too coarse to properly resolve the circulation patterns within the NECR. One of these models is the NCOM AMSEAS model, which is post-processed daily by CariCOOS and available at `http://www.caricoos.org/drupal/ncom_amseas`, including visualizations for the NECR. This model is produced by the Naval Research Laboratory and has a spatial resolution of 1/36 degree (3km) horizontal and 40 levels in the vertical. Sample output of this model for the NECR region is shown in Figure 3.1.

The second existing model is the CariCOOS Regional PR/USVI ROMS model, developed by CariCOOS under the leadership of Dr. Stefano Leonardi at UT Dallas and CariCOOS researchers at UPRM. This 3D ROMS model is forced by the NCOM AMSEAS model and is available operationally at `http://www.caricoos.org/drupal/roms`, and includes visualizations for the NECR region, as shown in Figure 3.2. We expect that further development of the ROMS model by CariCOOS will eventually allow the prediction of 3D current fields for the complex bathymetry of the NECR. At the moment, however, the model is not suitable for the present study.

3.1 High-resolution coastal circulation modeling in the NECR

The challenges of simulating the 3D current field in shallow regions with complex bathymetry such as the NECR, and taking into account the limited budget of the present study, has led to the implementation of a much simpler 2D model to simulate the hydrodynamics of the NECR. The selected model is CMS-Flow and the implementation of this model for the NECR is explained in detail in the next section.

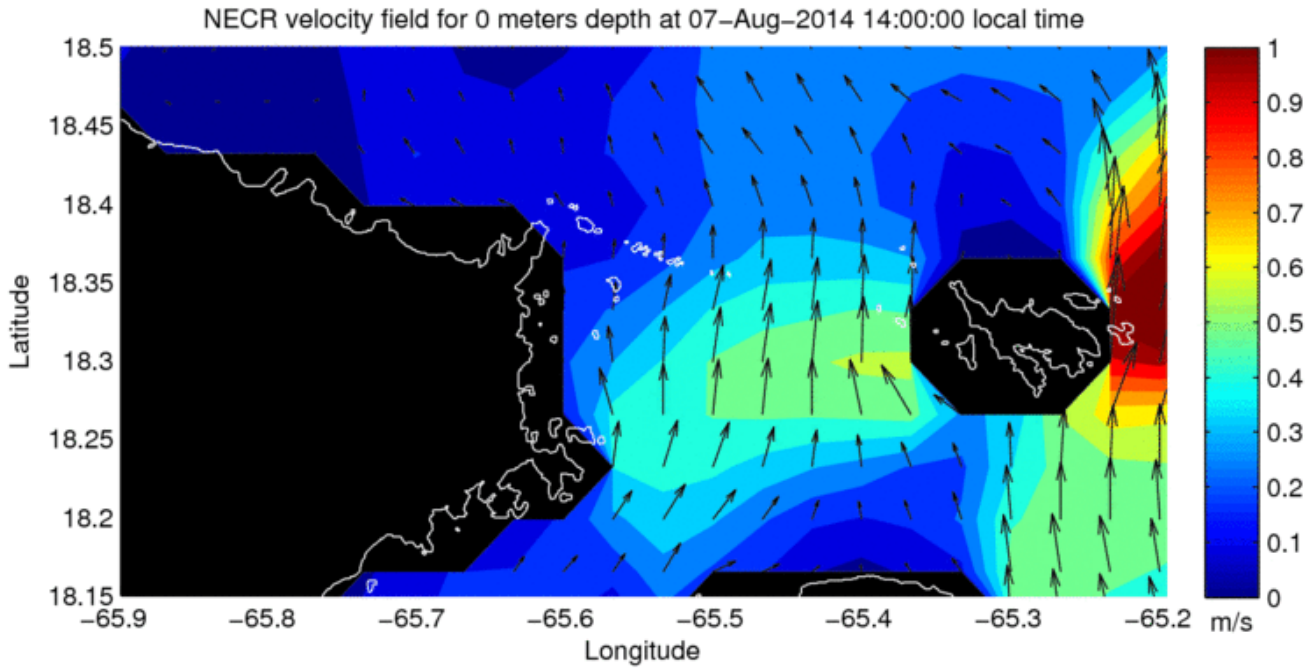

Figure 3.1: Sample output of the NCOM AMSEAS model for the NECR region, from `http://www.caricoos.org/drupal/ncom_amseas`.

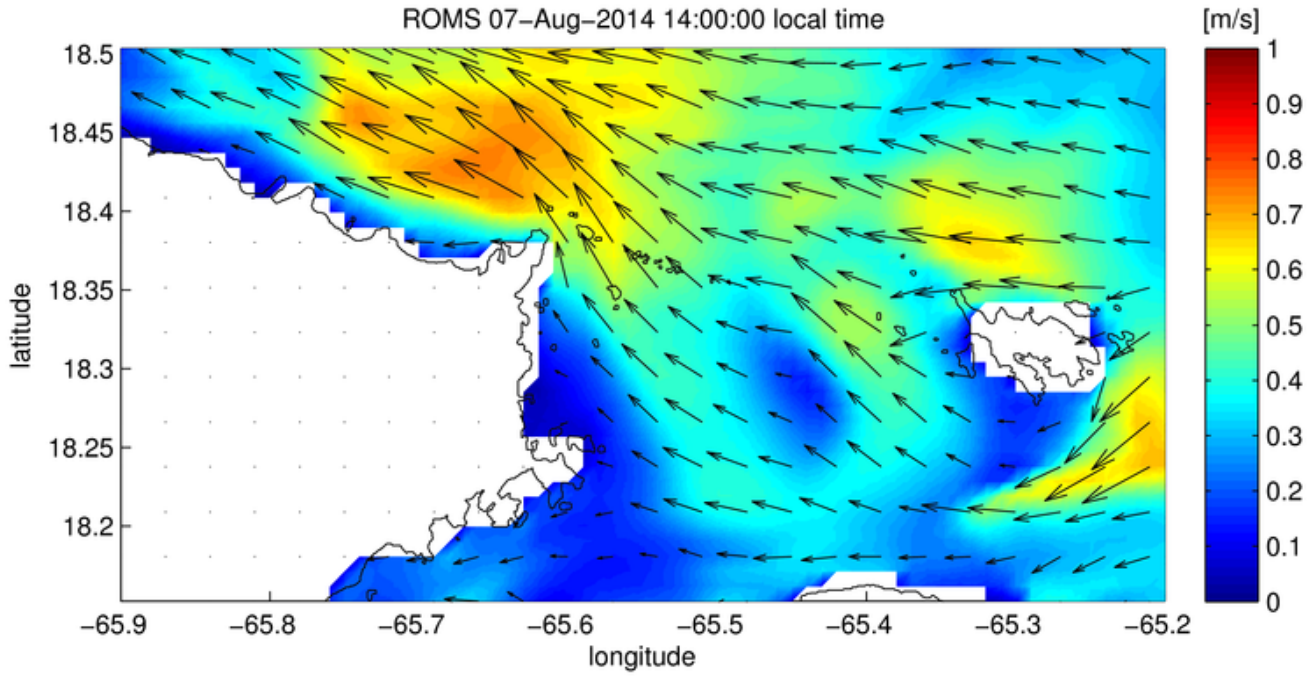

Figure 3.2: Sample output of the CariCOOS ROMS model for the NECR region, from `http://www.caricoos.org/drupal/roms`.

3.1.1 Model description

For the present study the selected model is the USACE Coastal Modeling System (CMS), which is an integrated model suite for the calculation of circulation, waves, sediment transport, pollutant mixing and morphology change (Buttolph et al., 2006). The CMS is composed of two separate models: CMS-Wave and CMS-Flow. CMS-wave is a spectral wave model used to simulate wave transformation and generation using the spectral action energy balance equations commonly used in phase-averaged wave models. CMS-Flow is used to simulate currents and sediment transport and has been applied extensively to solve problems in coastal hydrodynamics such as nearshore circulation (Coastal Processes Research Group, 2007), sediment transport and morphology change (Zarillo et al., 2009), river-ocean interactions (Lin et al., 2004), and to investigate the effect of wetland loss on the hydrodynamics of estuaries (Sanchez, 2008). For the present study, only CMS-Flow is used.

CMS-Flow uses a finite-volume approach to solving the depth-integrated two-dimensional equations of continuity and momentum. It solves these equations on an unstructured, multi-level telescoping quadtree (mass-conserving, implicit integration) rectangular mesh(Wu et al., 2010), which allows for local grid refinement in areas where high spatial gradients are expected, such as nearshore areas with complex bathymetry. CMS-Flow solves the depth-integrated momentum and continuity equations on 2D Cartesian coordinates (x, y, t):

$$\frac{\partial \vec{q}}{\partial t} + \vec{u} \cdot \vec{\nabla}_H \vec{q} + \frac{1}{2} g \vec{\nabla} (h + \eta)^2 = \vec{\nabla} \cdot (D \vec{\nabla} \vec{q}) + f \times \vec{q} - \vec{\tau}_b + \vec{\tau}_w + \vec{\tau}_S \tag{3.1}$$

$$\frac{\partial (h + \eta)}{\partial t} + \vec{\nabla}_H \cdot \vec{q} = 0 \tag{3.2}$$

where h is the still water level (SWL), η is the deviation of the water surface elevation from the SWL, $\vec{u}$ is the 2D velocity vector, $\vec{q} = (h + \eta)\vec{u}$ is the volume flow rate per unit width, D is the horizontal eddy viscosity coefficient (which may be spatially heterogeneous), f is the Coriolis parameter, and $\vec{\tau}_b$, $\vec{\tau}_w$ and $\vec{\tau}_S$ are the bottom shear stress, surface wind shear stress, and wave stress vectors, respectively. The surface wind stress is based on rough boundary layer theory. The bottom shear stress term takes into account the combined effect of waves and currents at an arbitrary angle, and the wave stresses are obtained from the divergence of the radiation stress tensor from classical momentum flux theory.

3.1.2 Model setup

A quadtree telescoping grid was developed for the NECR with resolution ranging from 300 meters in offshore areas to 25 meters in shallow regions with complex bathymetry. The grid is shown in Figure 3.3. The bathymetric data for the model grid was obtaimed from the USGS Digital Elevation Model (DEM) of Taylor et al. (2006) at a horizontal resolution of 10 meters.

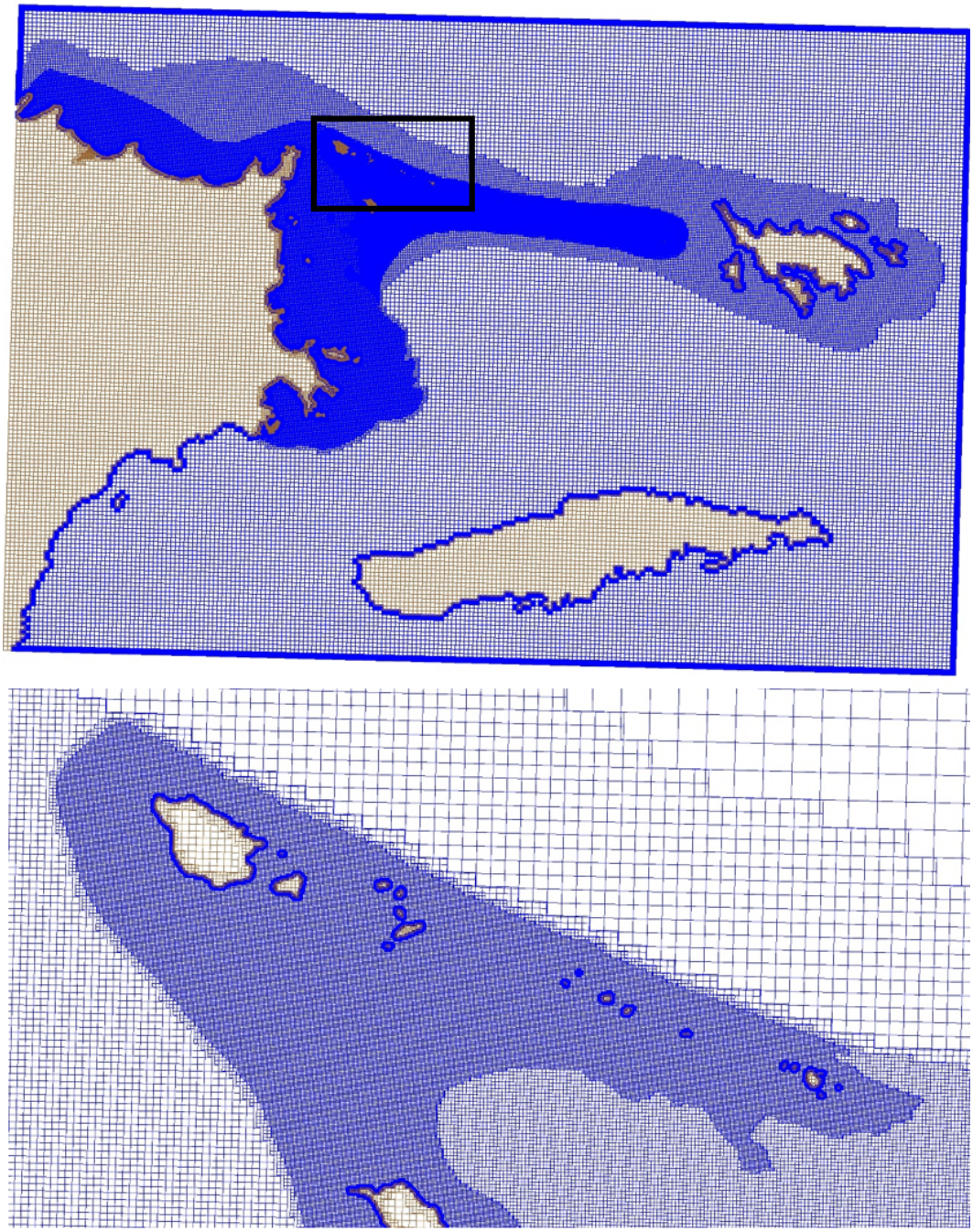

Figure 3.3: Telescoping CMS Flow grid developed for the present study with spatial resolution ranging from 300 meters in offshore areas to 25 meters in shallow regions with complex bathymetry. The top panel shows the complete grid while the lower panel shows a zoom (indicated by the black rectangle in the top panel) of the telescoping grid, showing the increased spatial resolution near the La Cordillera reefs.

The model was forced with tidal sea surface elevations along the model boundaries using the OTIS tidal database (`http://volkov.oce.orst.edu/tides/otis.html`). Surface wind forcing was obtained from the National Weather Service National Digital Forecast Database. For the present study the model was run for one month, from November 1-30 2013.

3.1.3 Model output

Snapshots of the model output are shown in Figures 3.4 through 3.7. Figure 3.4 shows a typical vector field during flood tide on November 12 2013 at 3 AM LST, while Figure 3.5 shows an example of the current velocity field during ebb tide at 9 AM LST the same day. The strongest tidal currents occur near the La Cordillera reefs and at the San Juan Passage between Las Cabezas de San Juan and Cayo Icacos. Near Culebra, the strongest currents (up to 1 ms^{-1}) occur to the east of the main island of Culebra at the Canal de Cayo Norte and the Canal de Culebrita. Strong tidal currents also occur west of Culebra at the Luis Peña Canal. Figures 3.6 and 3.7 show a zoom of the typical vector fields around Cayo Icacos and Palomino Island for flood and ebb tide for the same time as Figures 3.4 and 3.5, respectively.

In order to determine whether the vector fields shown in Figures 3.4 through 3.7 are representative of the current dynamics in the NECR, in the next section the model output is validated with ocean observing assets within the NECR.

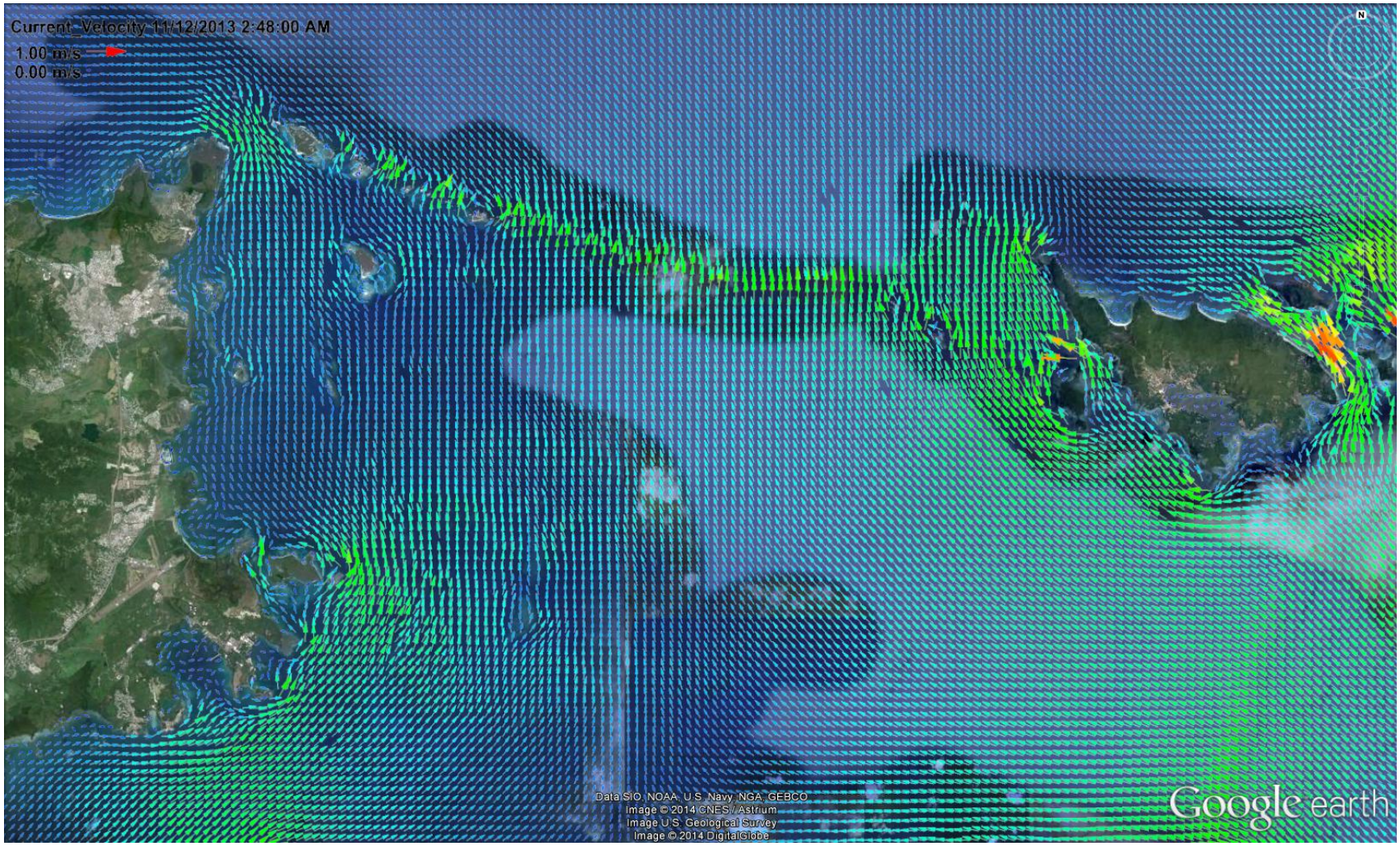

Figure 3.4: Typical current velocity field during flood tide, shown here on November 12 2014 at 3 AM LST.

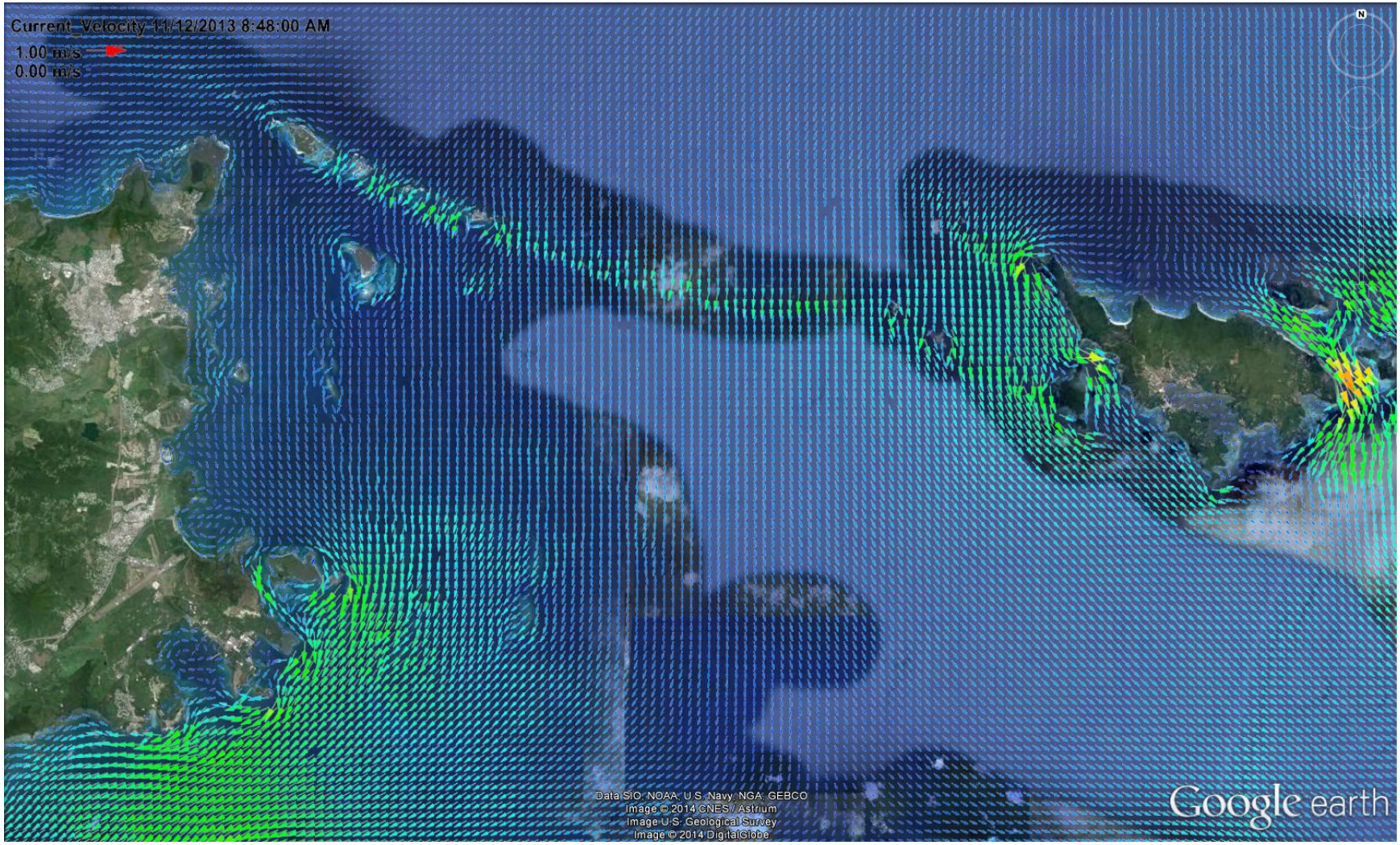

Figure 3.5: Typical current velocity field during ebb tide, shown here on November 12 2014 at 9 AM LST.

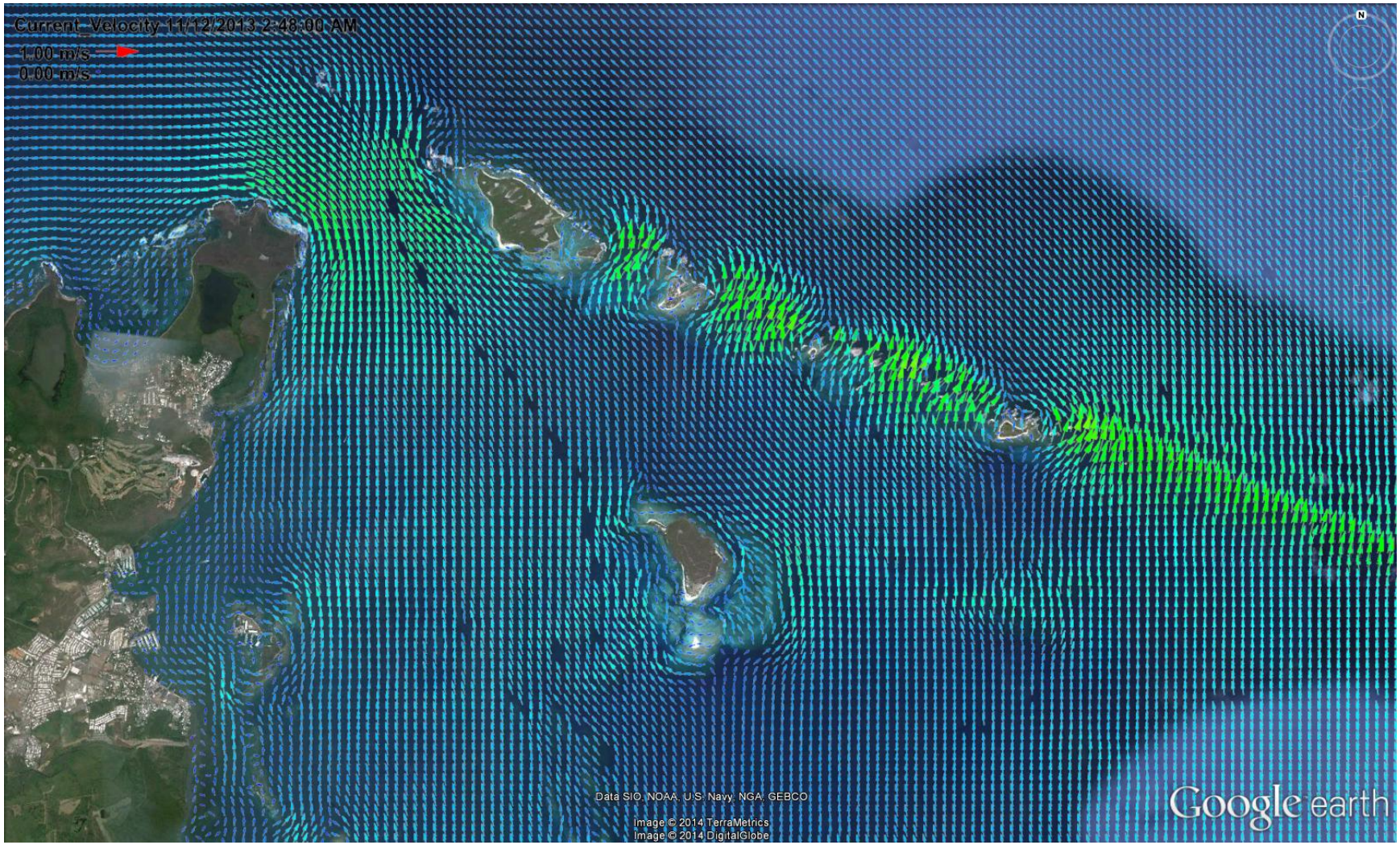

Figure 3.6: Typical current velocity field during flood tide near Icaco, shown here on November 12 2014 at 3 AM LST.

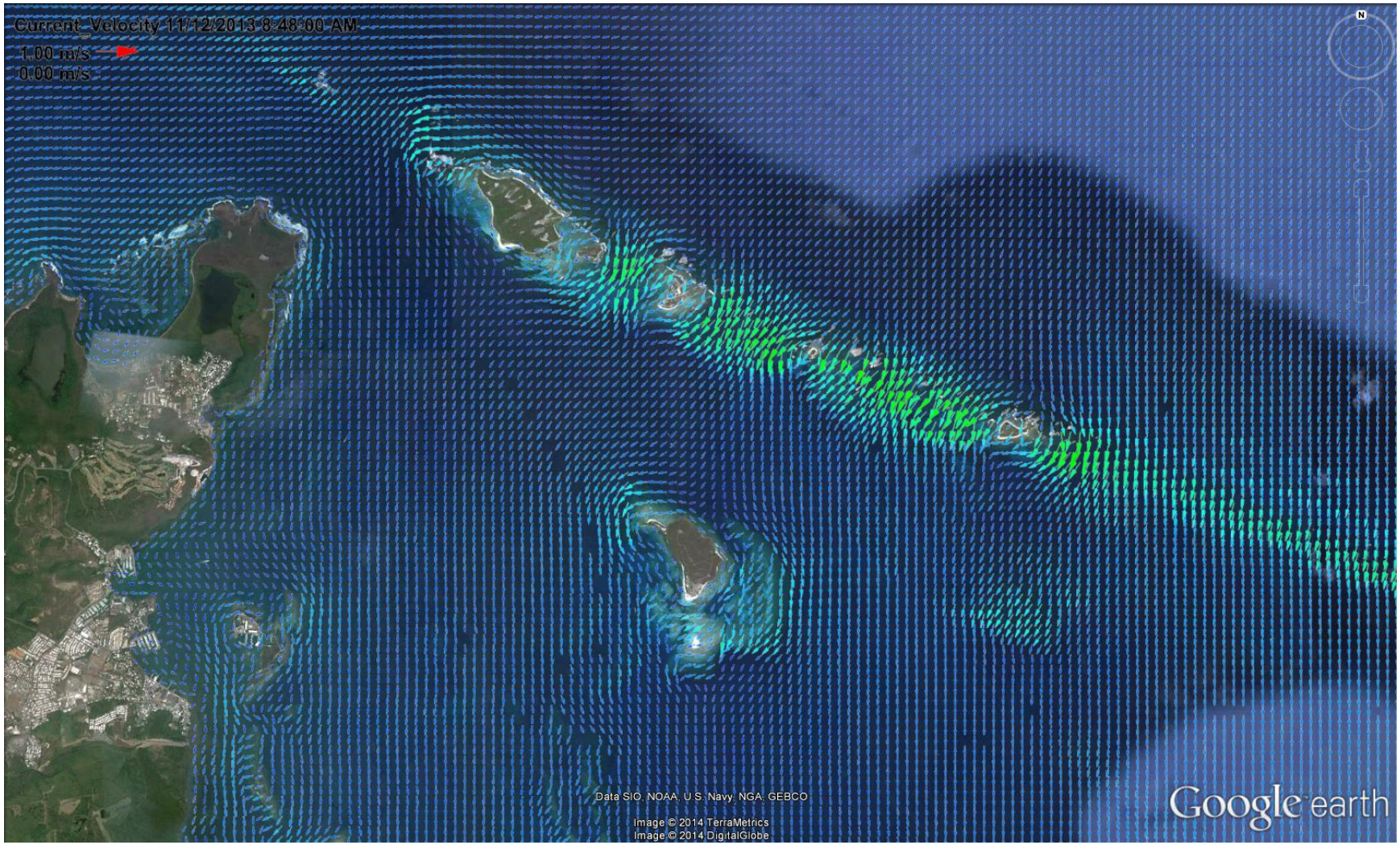

Figure 3.7: Typical current velocity field during ebb tide near Icaco, shown here on November 12 2014 at 9 AM LST.

3.1.4 Model validation

To ensure correct application of boundary conditions and realistic representation of the tidal elevation within the NECR, model output data was compared with the Fajardo tide gauge (NOS water level station 9753216), as shown in Figure 3.8. Excellent agreement is found between the observed (red line) and predicted (blue line) sea surface elevation at the tide gauge location, indicating excellent model performance in reproducing tidal elevation dynamics within the NECR.

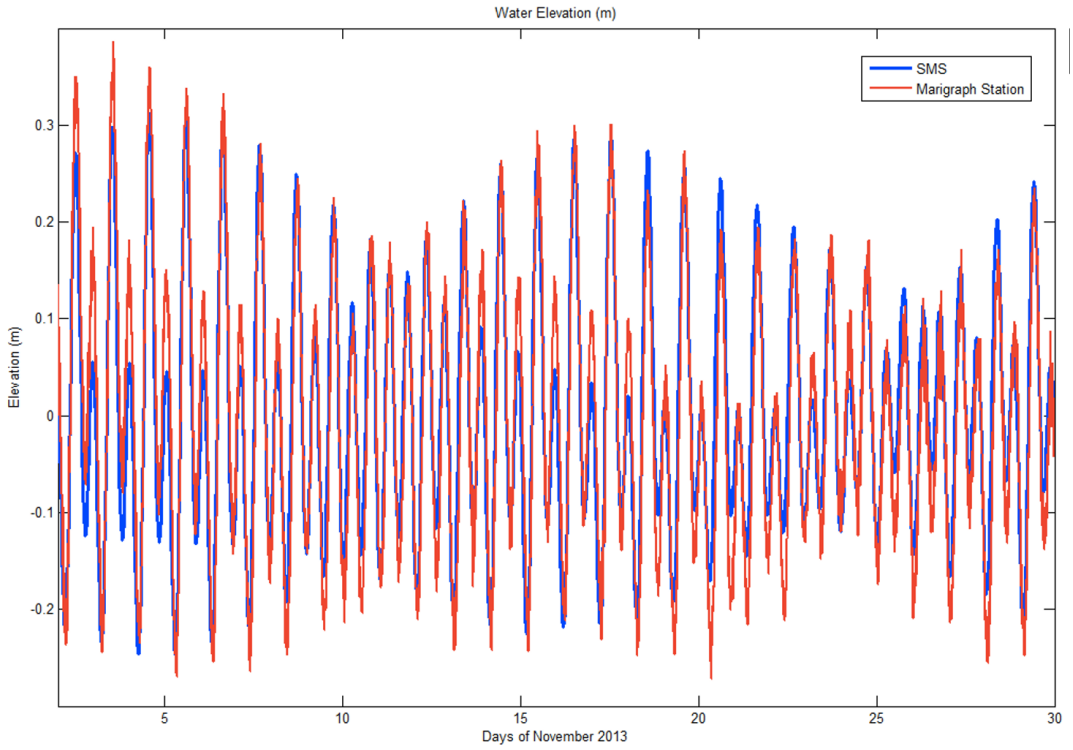

Figure 3.8: Comparison between simulated sea surface elevation (blue line) vs. observed sea surface elevation at the Fajardo NOS tide gauge.

To validate the current velocity results, model output was compared to current velocity observations at CariCOOS Data Buoy E, located within the NECR at Latitude 18^o 15.58'N, Longitude 65^o 27.45'W. The location of the buoy is shown in Figure 3.9. The buoy is equipped with a suite of oceanographic sensors and for the purpose of this study only data from the current meters are used. The mooring / instrument configuration of the buoy is shown in Figure 3.10. The buoy is able to measure the full water column velocity profile. The present study uses a 2D (depth-integrated) model and as such, only the depth-integrated velocities observed at the buoy are compared with the model predictions.

Results of the time-series comparison are shown in Figure 3.11. The top panel shows a comparison between observed (red line) and model-predicted (blue line) east-west (U) velocity component, while

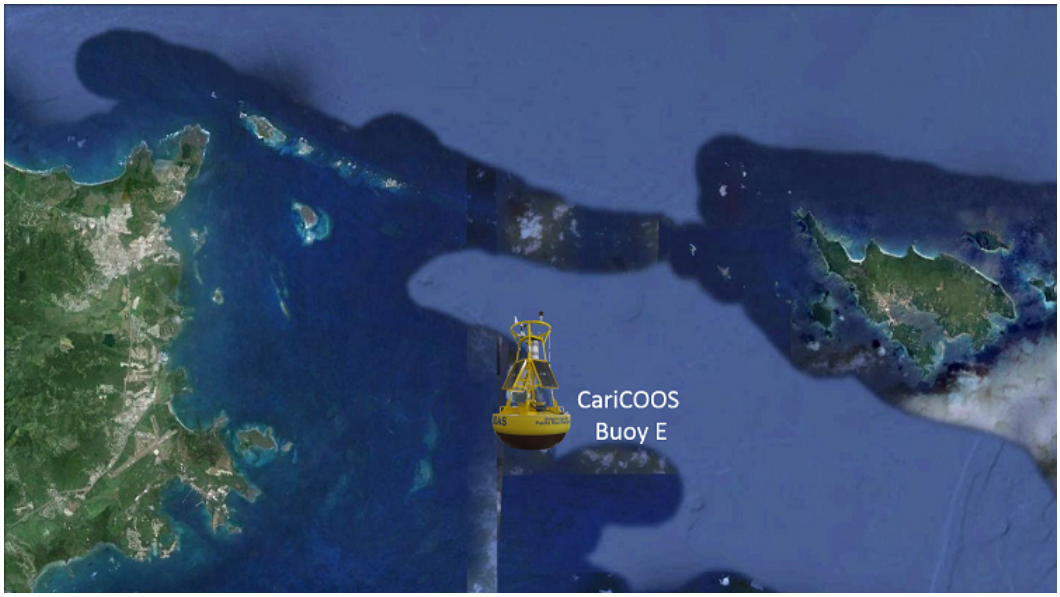

Figure 3.9: Location of CariCOOS Data Buoy E within the NECR.

the lower panel shows the comparison for the north-south velocity component. The model performs very well for most of the month-long time series, with the largest differences occurring during periods of strong winds as measured by the buoy. These differences may be due to the coarse nature of the wind models used to provide wind surface boundary conditions to CMS Flow. The performance of the model, however, is satisfactory and allows for the use of the model to examine the spatial structure of the current vector field statistics throughout the NECR. This analysis is provided in the next section.

3.2 Spatial distribution of current speed statistics

Using one month of high resolution numerical model output for the NECR, the spatial distribution of the current velocity structure can be obtained by computing the statistics of the current velocities at each model grid point. Figure 3.12 shows the maximum current magnitude simulated during November 2013. Note that the model only takes into account tide and wind driven currents, and that wave-driven currents during large wave events may be stronger than the tide and wind driven currents at certain locations with wave breaking and strong wave refraction. The strongest maximum currents, in excess of 1 ms^{-1}, within the NECR can be found to the east of the main island of Culebra at the Canal de Cayo Norte and the Canal de Culebrita, as well as west of Culebra at the Luis Peña Canal. Very strong currents are also evident in the Vieques Passage near Punta Arenas, west of Vieques. Closer to Fajardo, strong currents (although weaker than those at Culebra) are found and the reef passages of the La Cordillera Reefs Natural Reserve as well as the passage between Las Cabezas de San Juan and Cayo Icacos. Figure 3.13 shows the mean currents during November 2013 and show the same spatial distribution as the maximum

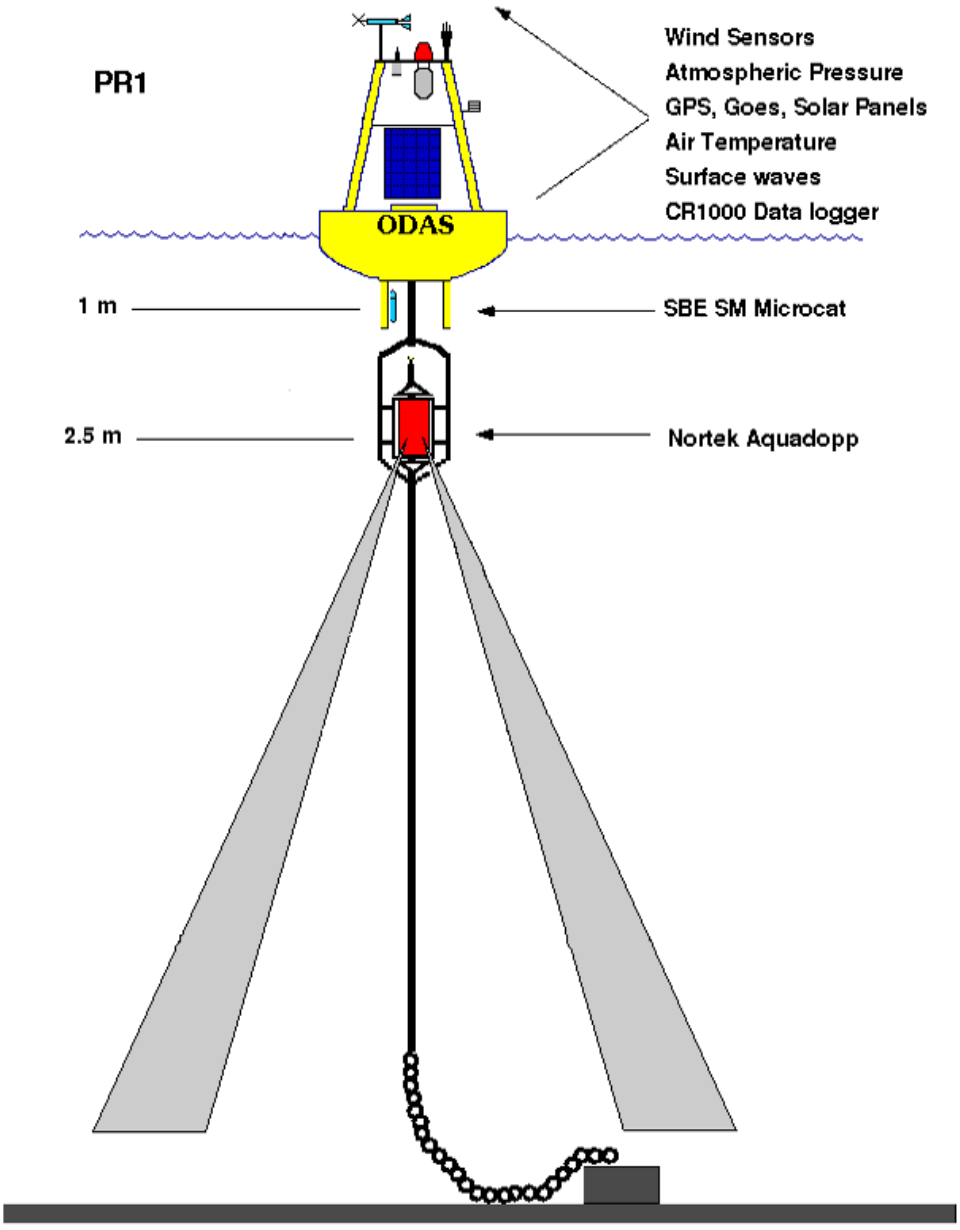

Figure 3.10: Instrument and mooring configuration of CariCOOS Data Buoy E.

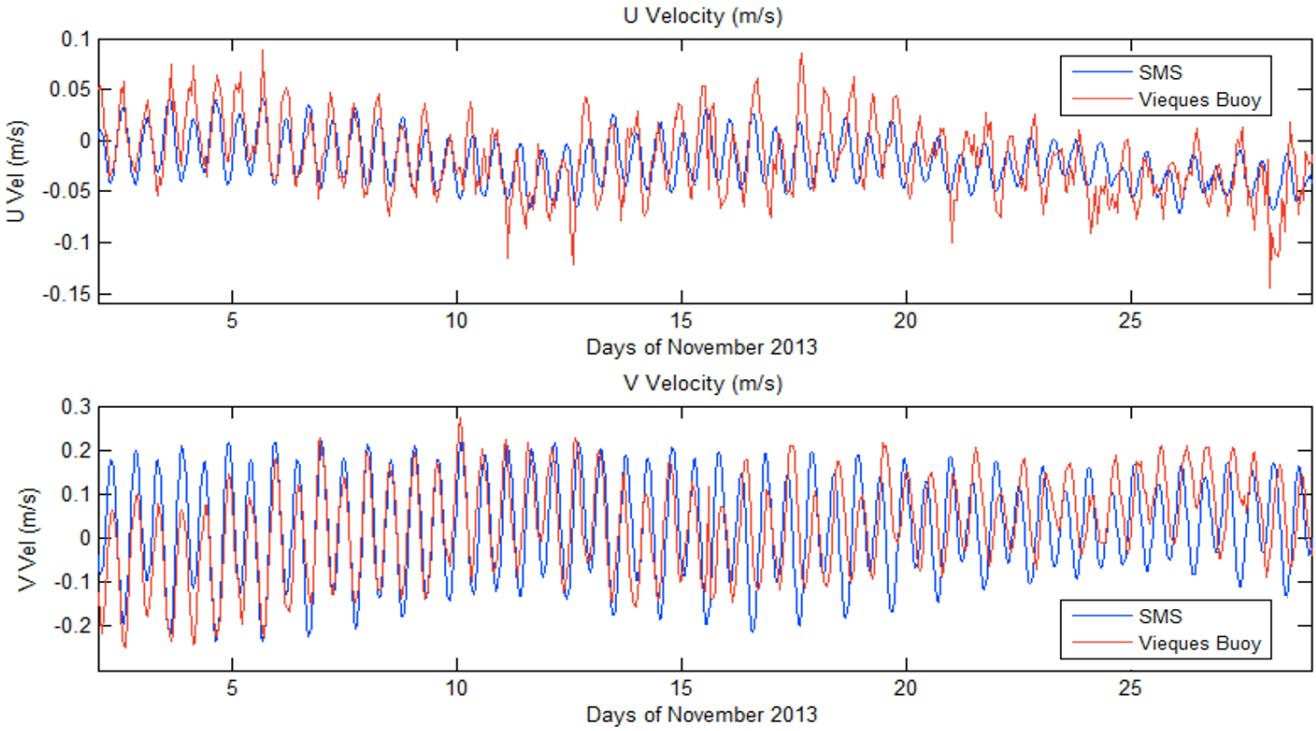

Figure 3.11: test

currents discussed above.

Figures 3.14 and 3.15 show the maximum and mean currents during November 2013, respectively, focusing on the La Cordillera Reefs Natural Reserve. Note the stronger currents in the shallow Cordillera region, as well as the hotspots of strong currents in the passages between islands within La Cordillera such as Cayo Diablo, La Blanquilla, Cayo Lobos, etc. This small scale structure of the maximum and time-averaged current velocity field is better shown in Figures 3.16 and 3.17 which focus on the areas near Fajardo, Cayo Icacos and Palominos. Again, note the spatial heterogeneity of the current velocity spatial structure. What role this complex spatial structure plays in the distribution of endangered coral species such as elkhorn coral within the NECR remains to be determined.

These datasets have been shared with the NOAA Biogeography Group for inclusion into their online NECR spatial database. It is expected that this data will be useful for marine spatial planning efforts within the NECR.

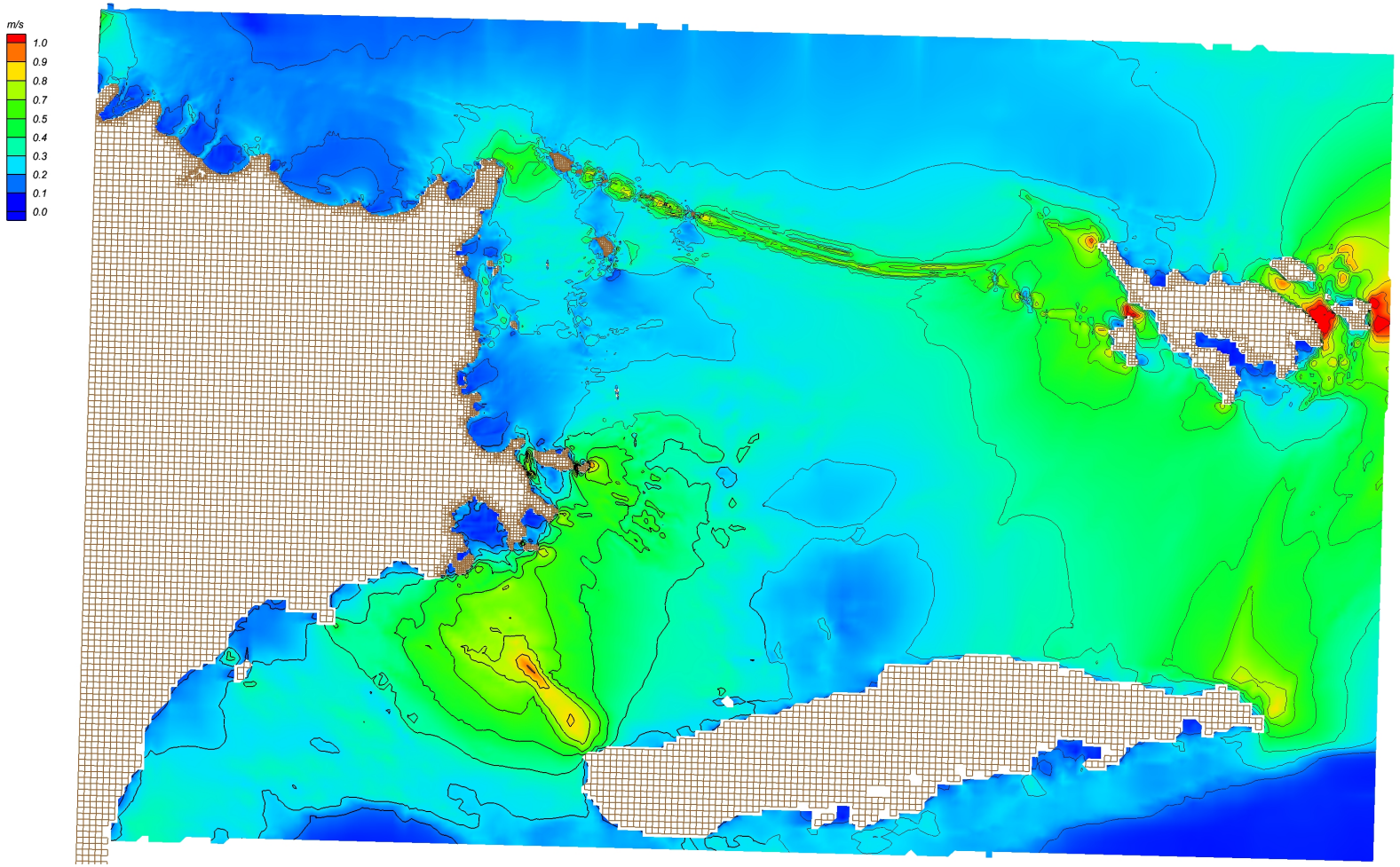

Figure 3.12: Zoom of maximum tide and wind driven currents for the NECR region during November 2013

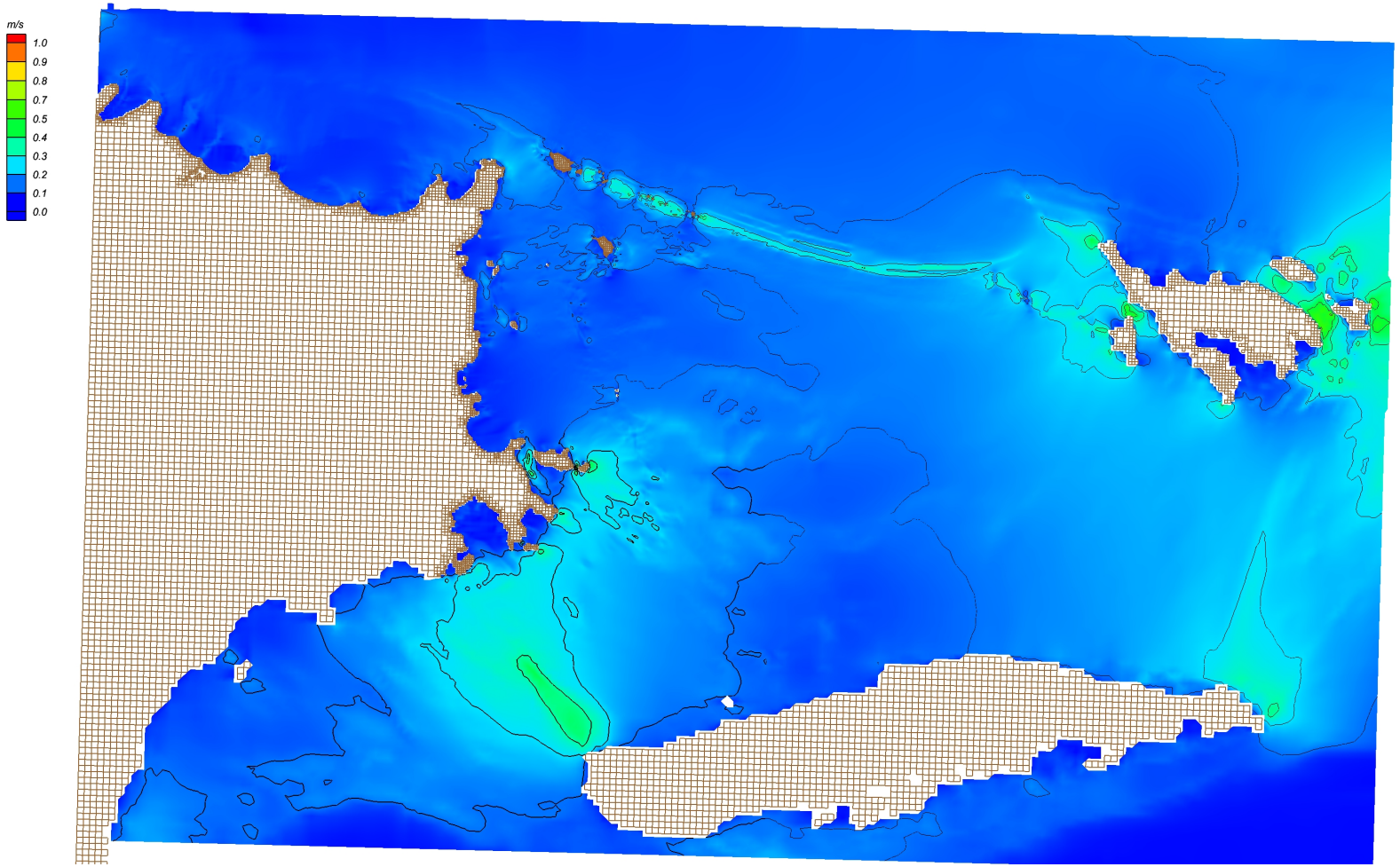

Figure 3.13: Zoom of average tide and wind driven currents for the NECR region during November 2013

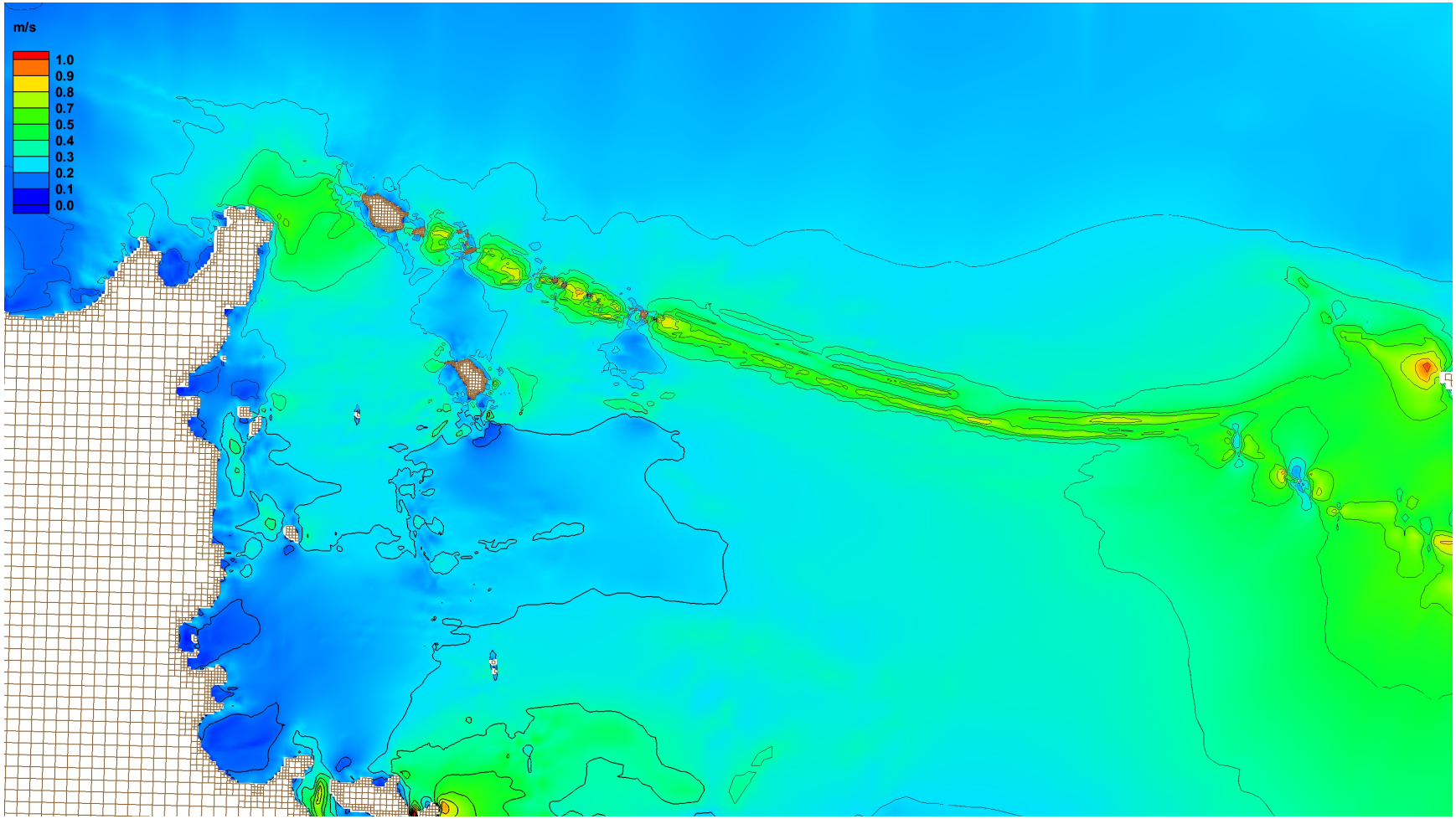

Figure 3.14: Zoom of maximum tide and wind driven currents for La Cordillera region during November 2013

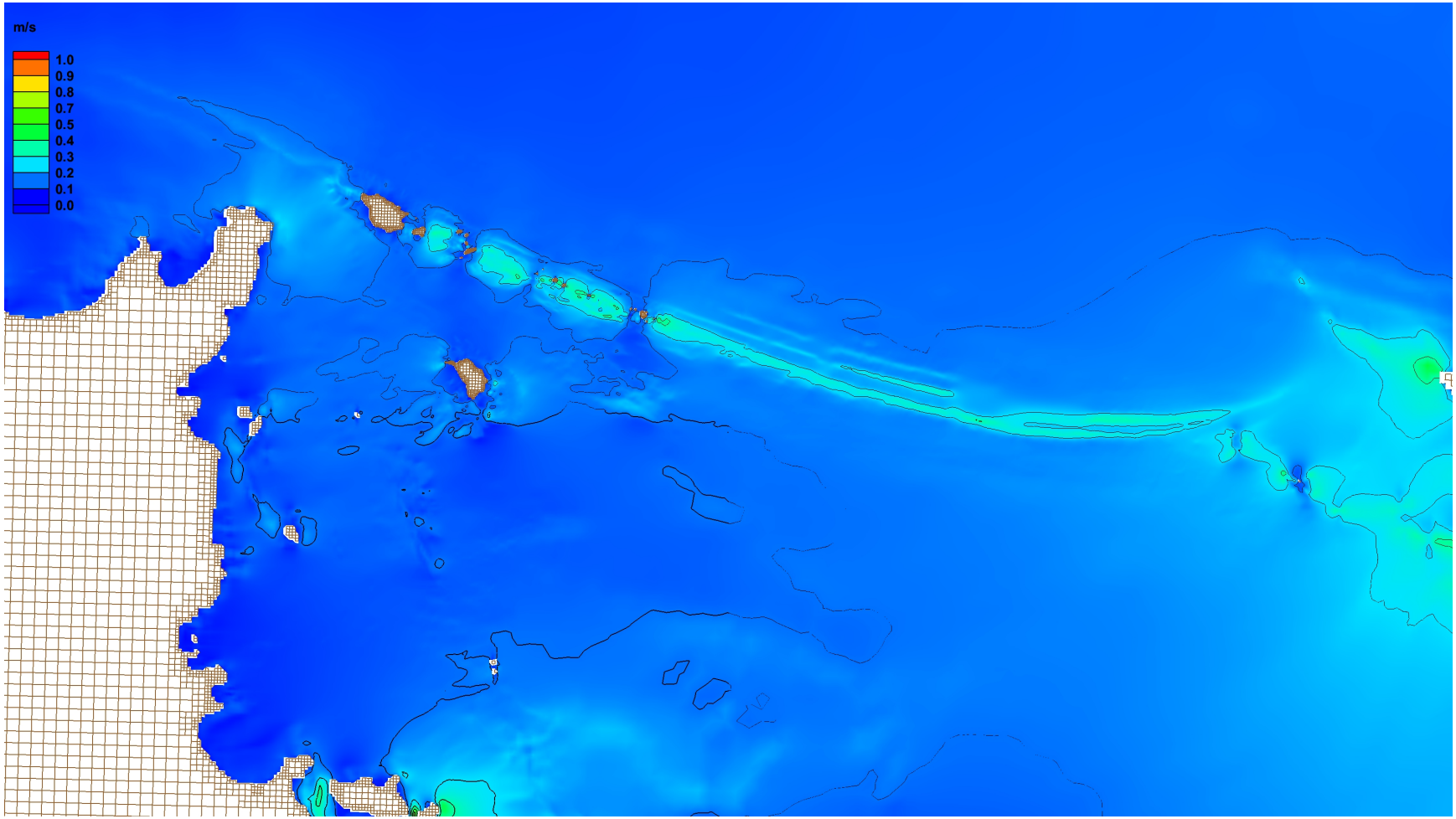

Figure 3.15: Zoom of average tide and wind driven currents for La Cordillera region during November 2013

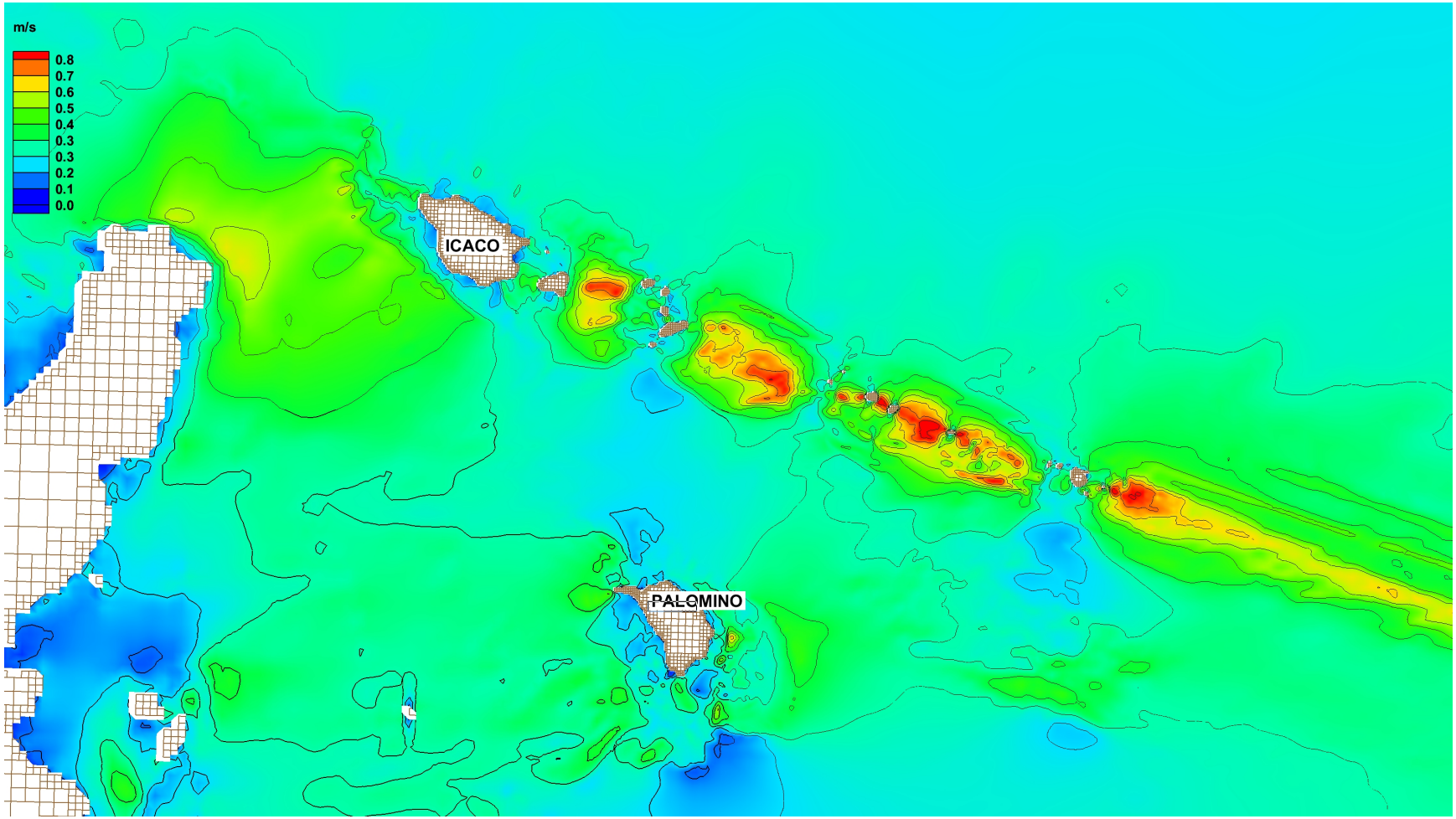

Figure 3.16: Zoom of maximum tide and wind driven currents near Icaco and Palomino islands during November 2013

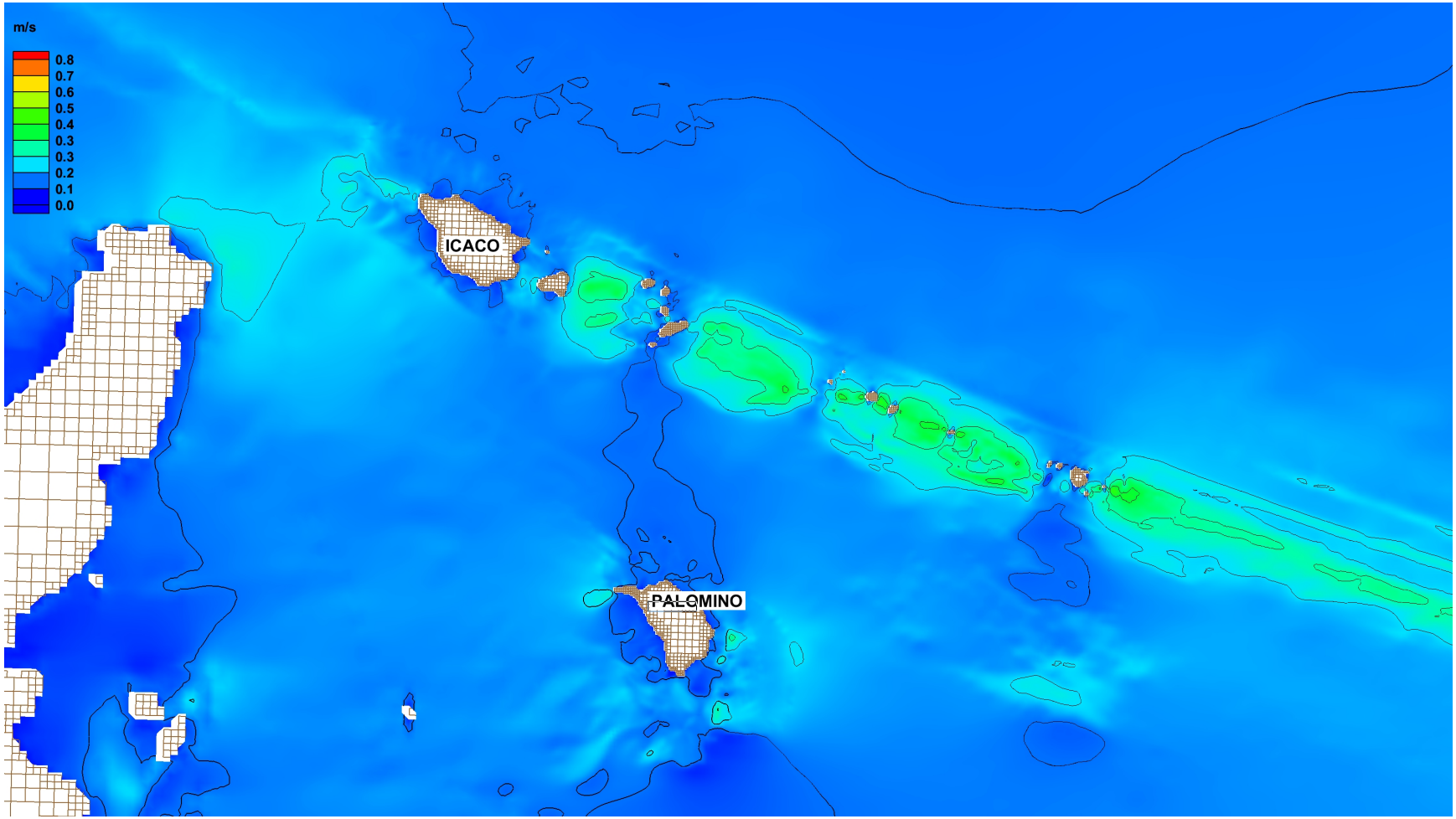

Figure 3.17: Zoom of average tide and wind driven currents near Icaco and Palomino islands during November 2013

Chapter 4

Preliminary particle transport modeling (PTM) in the NECR

As part of the present study, preliminary simulations of particle trajectories have been conducted using the USACE Particle Tracking Model (PTM). The PTM is a Lagrangian model which simulates the transport of particles with specified size, specific gravity, grain size distribution and fall velocity characteristics, etc. The PTM uses an existing hydrodynamic simulation to drive the particle tracking algorithms. In the case of the present study, the hydrodynamic forcing to the PTM is provided by the CMS-Flow simulations for the NECR for November 2013, which were described and validated in the preceding chapter. The use of 2D models for particle tracking purposes is acceptable for shallow, well mixed nearshore and continental shelf areas. Numerical models similar to CMS Flow such as ADCIRC have been used to study oil dispersal in coastal areas which good results (Dietrich et al., 2012). PTM has been used extensively for similar applications and, for example, has been used to study the exposure of critical coral reef areas to sediment suspension from dredging activities (King et al., 2012). Technical details of the PTM model may be found in MacDonald et al. (2006).

For the present study, two preliminary PTM simulations were performed, both assuming that the released material were neutrally buoyant particles:

1. A 36 hour long release consisting of a line source at Las Croabas, starting at 2 AM on November 3, 2013 and lasting through 12 PM November 4, 2013 as shown in Figure 4.1. The results from this simulation are shown in Figures 4.2 through 4.7 for select time steps.

2. A 48 hour long release consisting of two point sources starting at 2 AM on November 2, 2013 and lasting through 2 AM November 4, 2013. One source was located in the shallow reef area southeast of Cayo Icacos and the other source northwest of Cayo Lobos, as shown in Figure 4.1. The results from this simulation are shown in Figures 4.8 through 4.17 for select time steps.

While there is no Lagrangian data to validate the predictions of particle dispersal, Figure 4.18 shows

Figure 4.1: Locations of the point sources near Cayo Icacos and Cayo Lobos and the line source at Las Croabas.

a visual comparison of the computed particle positions from the Las Croabas particle release (top panel) and an aerial picture obtained from Google Earth showing a suspended sediment plume (bottom panel). Note the tendency of the plume to remain attached to the coastal boundary layer.

The PTM simulations presented herein are only two preliminary simulations with arbitrary durations and source locations. Future simulations should include input from coastal managers working within the NECR in order to use the simulations to address larval connectivity or sediment loading issues within the NECR.

Figure 4.2: Location of neutrally boyant particle (in yellow) after the line source release, on November 3, 2013 at 2 AM.

Figure 4.3: Location of neutrally boyant particle (in yellow) after the line source release, on November 3, 2013 at 6 AM.

Figure 4.4: Location of neutrally boyant particle (in yellow) after the line source release, on November 3, 2013 at 12 PM.

Figure 4.5: Location of neutrally boyant particle (in yellow) after the line source release, on November 3, 2013 at 6 PM.

Figure 4.6: Location of neutrally boyant particle (in yellow) after the line source release, on November 4, 2013 at 12 AM.

Figure 4.7: Location of neutrally boyant particle (in yellow) after the line source release, on November 4, 2013 at 6 AM.

Figure 4.8: Particle positions on November 2 2013 at 7:33 AM from point source releases at Cayo Icaco and Cayo Lobos.

Figure 4.9: Particle positions on November 2 2013 at 11:33 AM from point source releases at Cayo Icaco and Cayo Lobos.

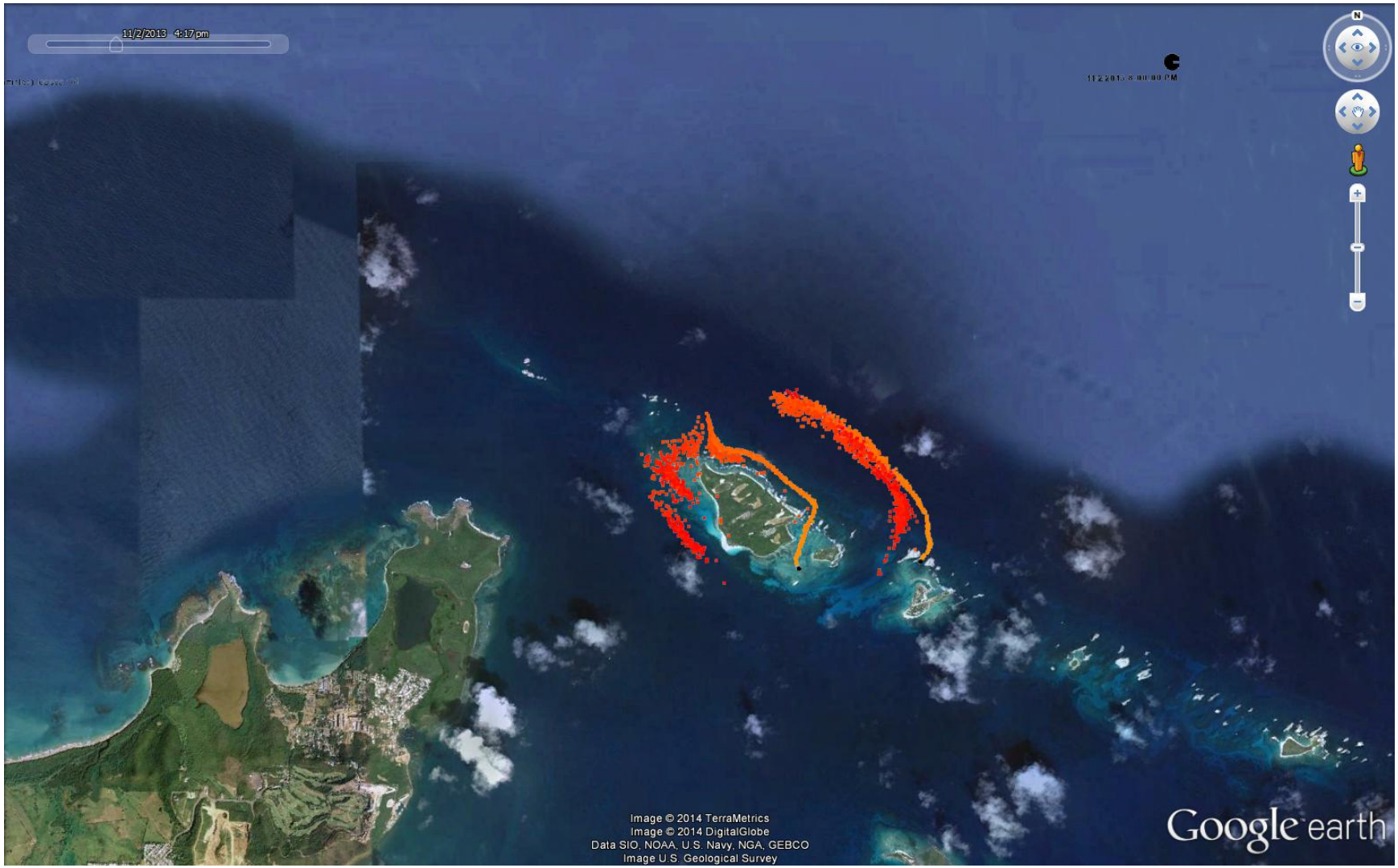

Figure 4.10: Particle positions on November 2 2013 at 4:17 PM from point source releases at Cayo Icaco and Cayo Lobos.

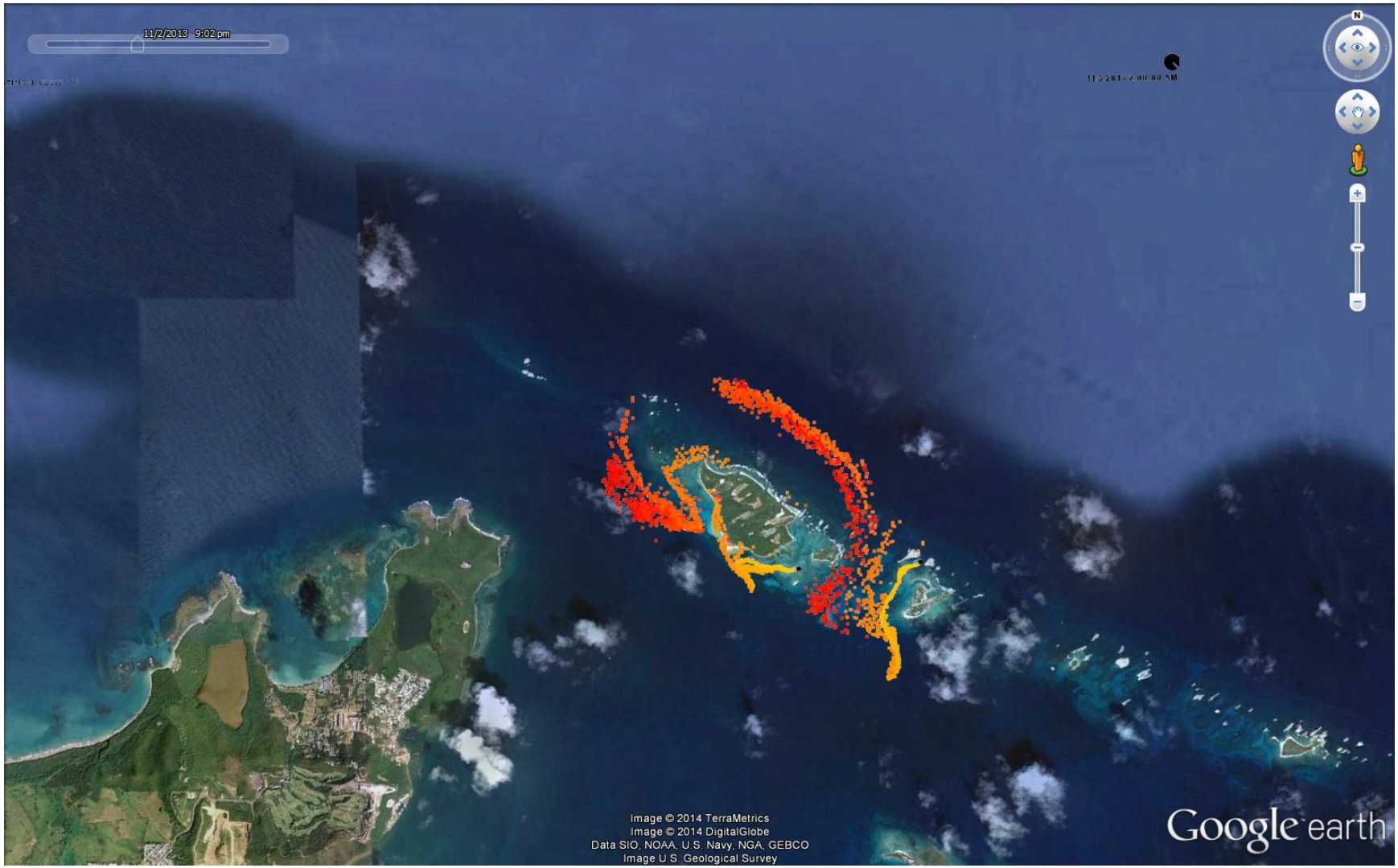

Figure 4.11: Particle positions on November 2 2013 at 9:02 PM from point source releases at Cayo Icaco and Cayo Lobos.

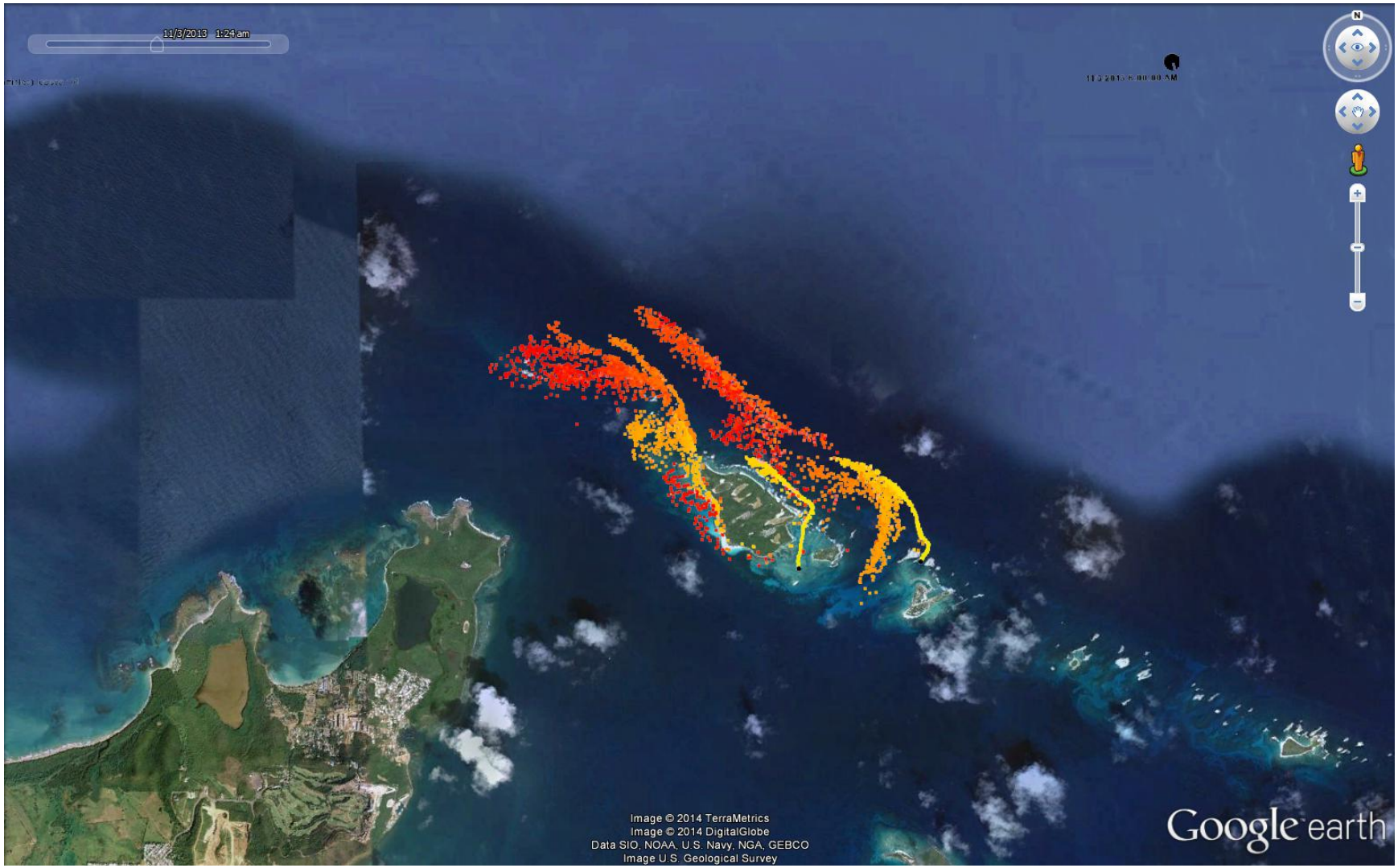

Figure 4.12: Particle positions on November 3 2013 at 1:24 AM from point source releases at Cayo Icaco and Cayo Lobos.

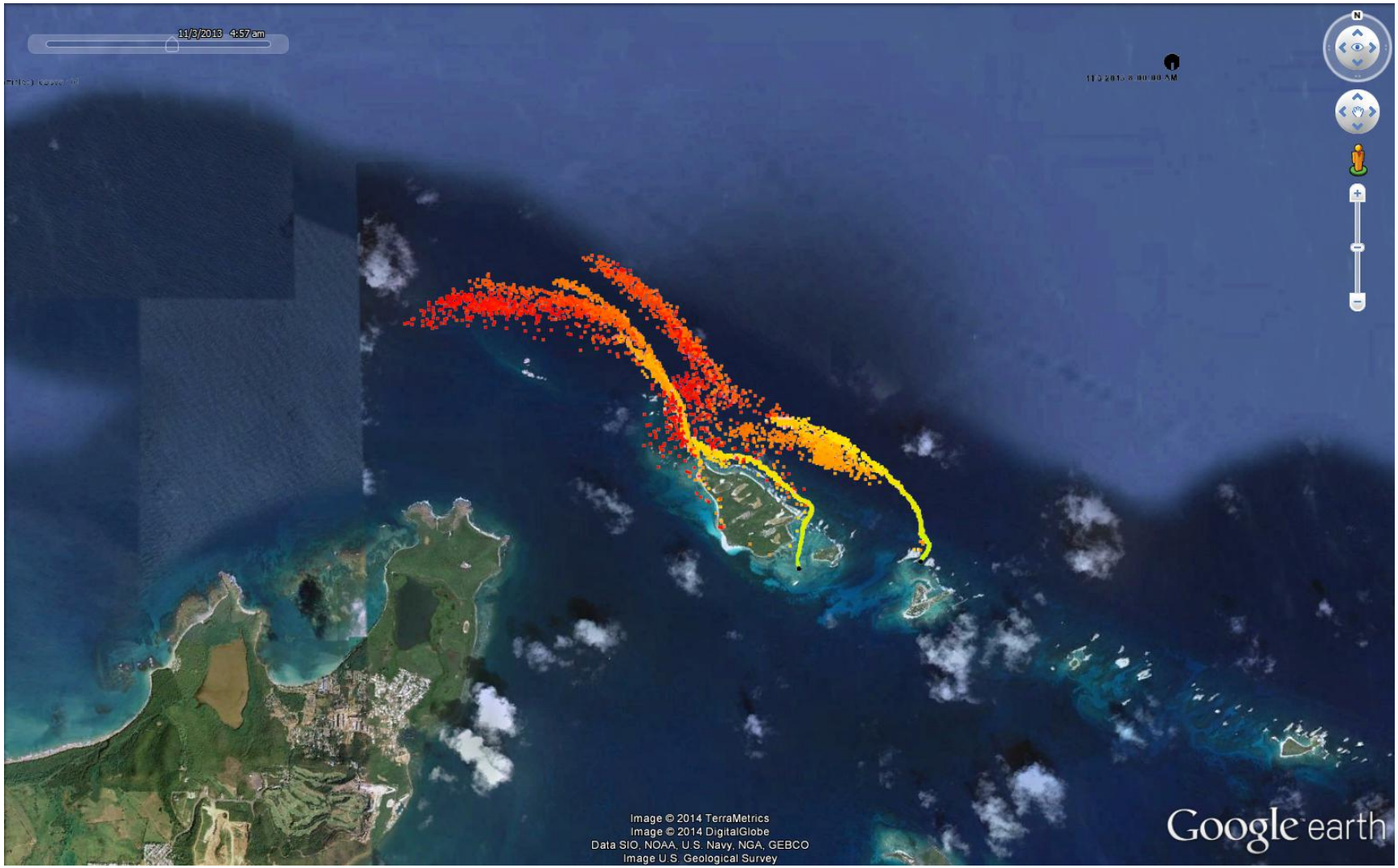

Figure 4.13: Particle positions on November 3 2013 at 4:57 AM from point source releases at Cayo Icaco and Cayo Lobos.

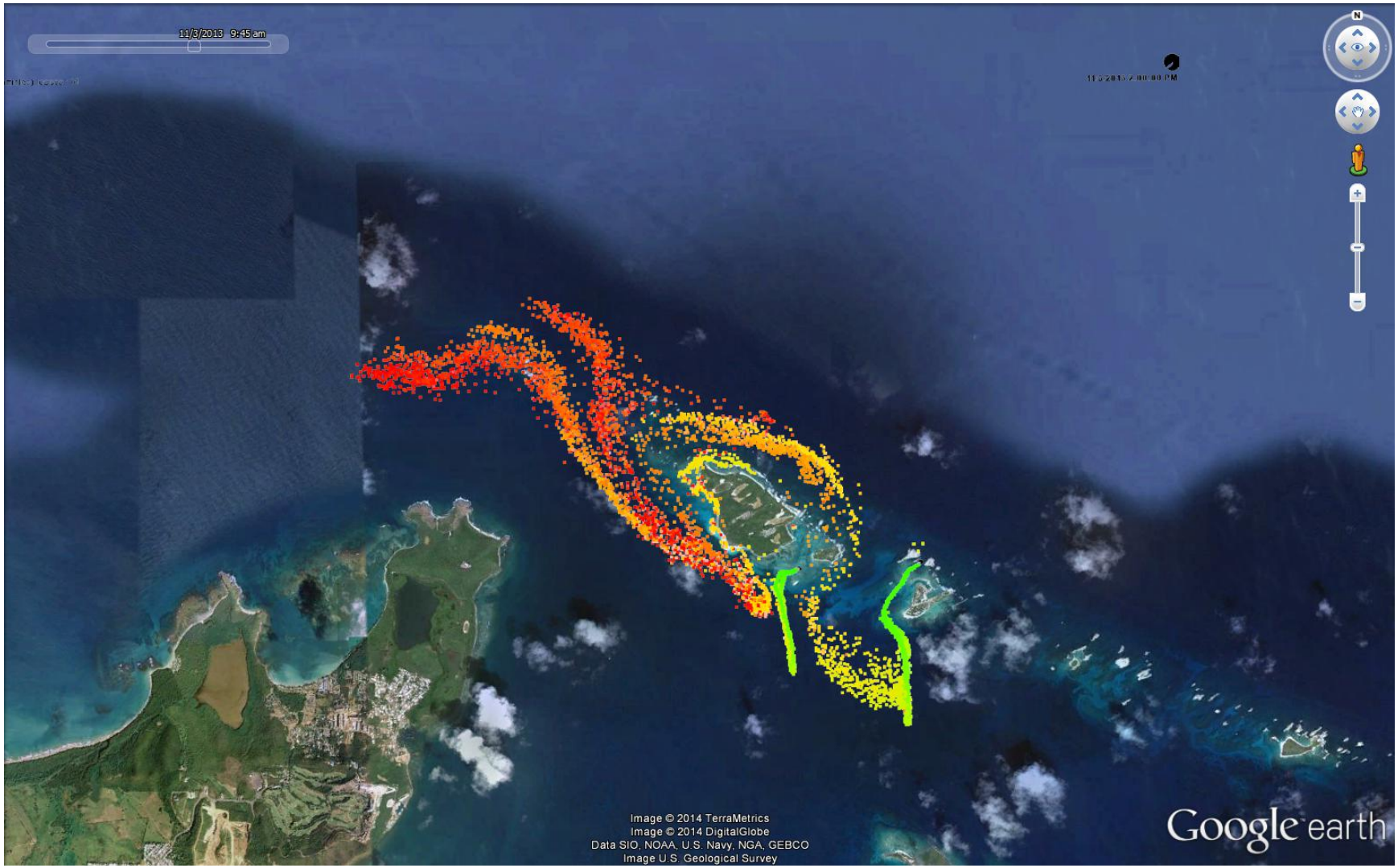

Figure 4.14: Particle positions on November 3 2013 at 9:45 AM from point source releases at Cayo Icaco and Cayo Lobos.

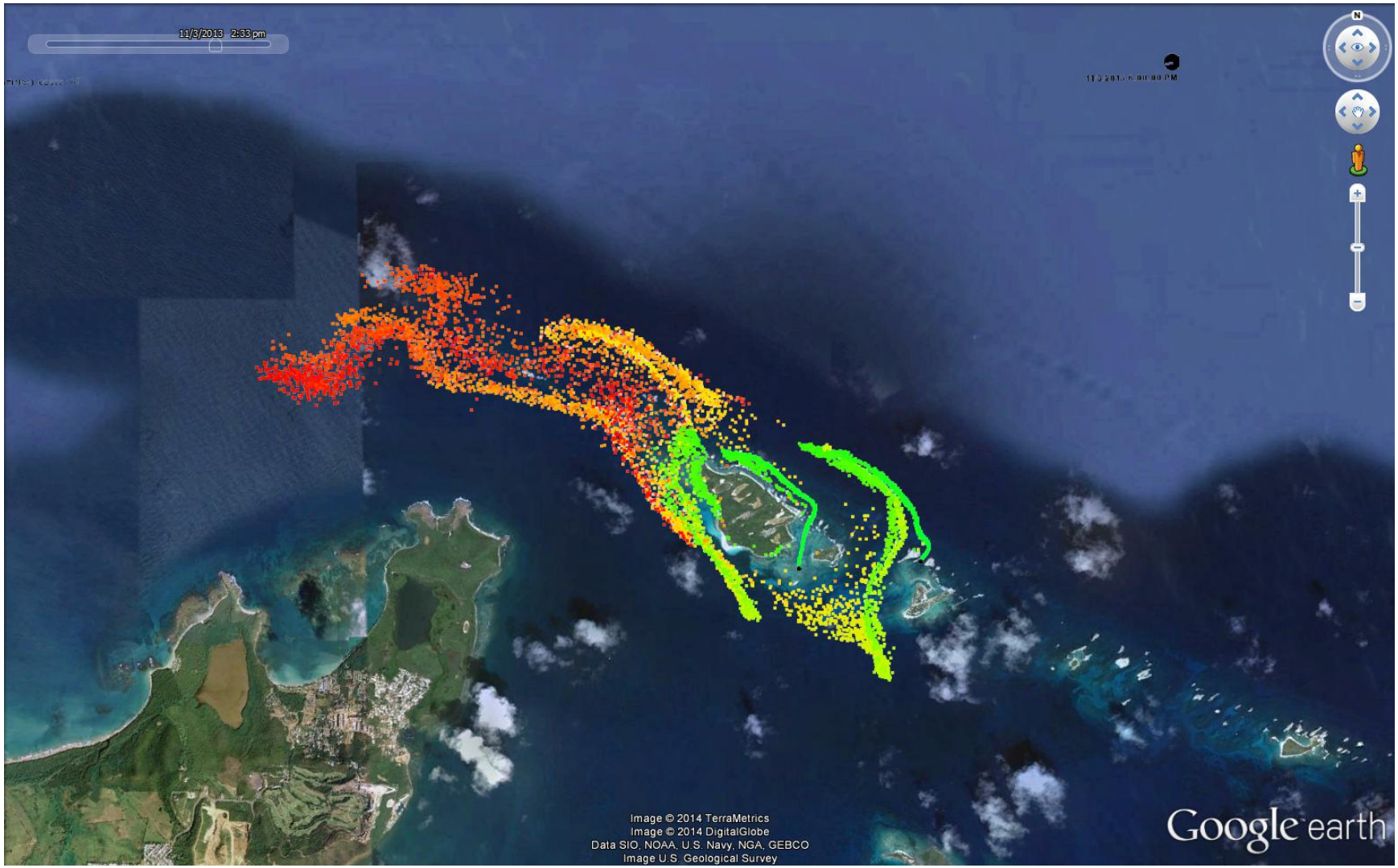

Figure 4.15: Particle positions on November 3 2013 at 2:33 PM from point source releases at Cayo Icaco and Cayo Lobos.

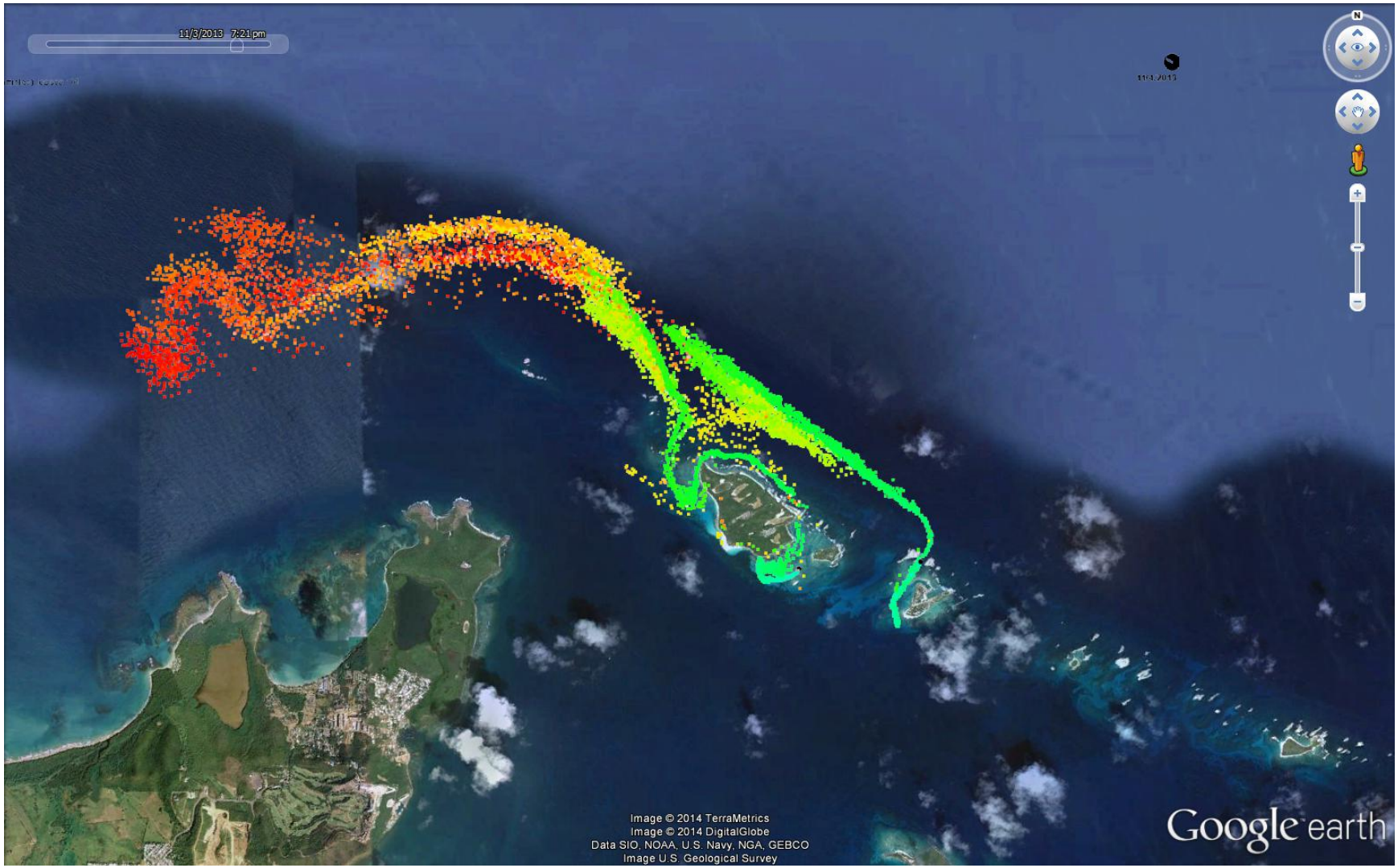

Figure 4.16: Particle positions on November 3 2013 at 7:21 PM from point source releases at Cayo Icaco and Cayo Lobos.

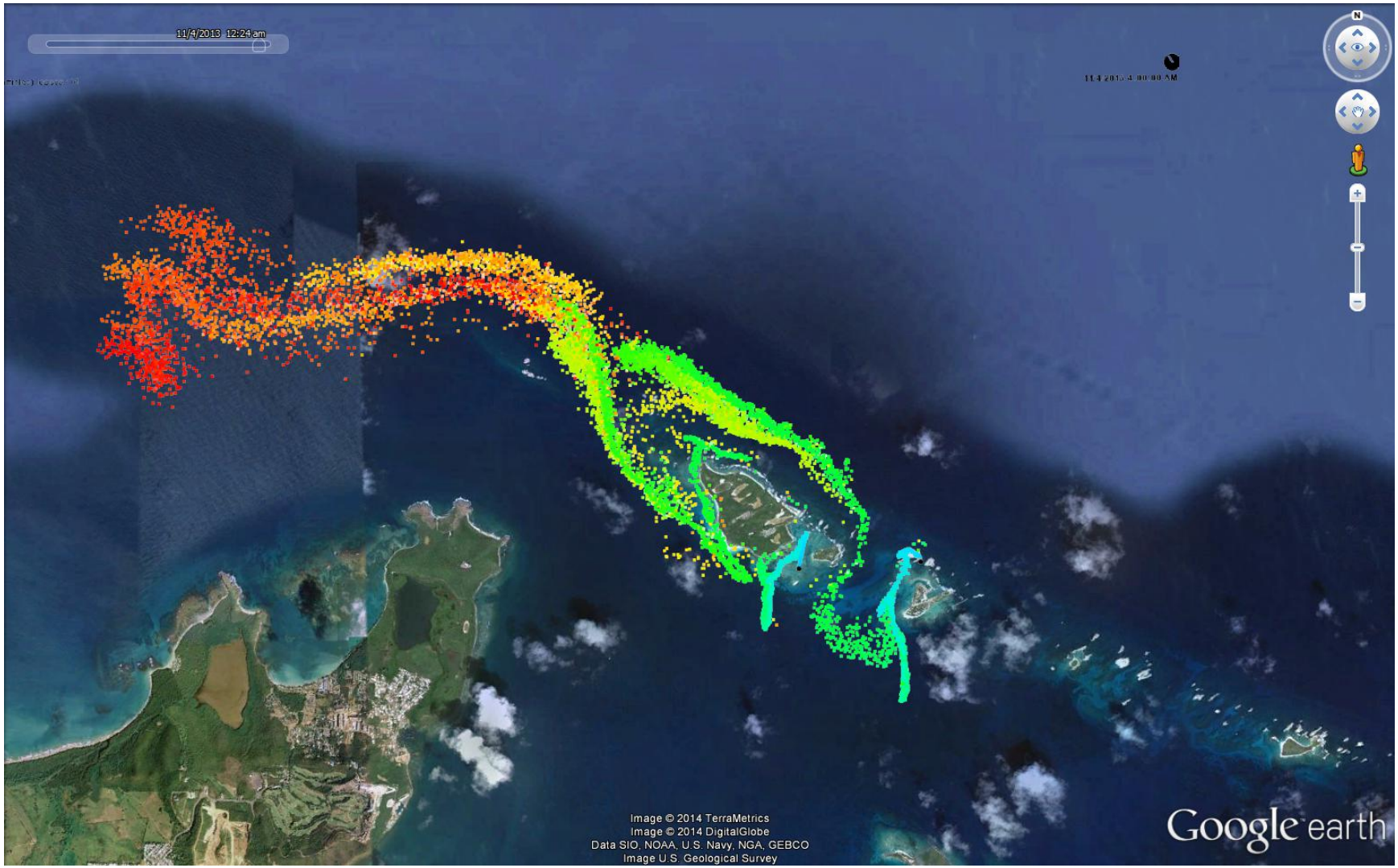

Figure 4.17: Particle positions on November 4 2013 at 12:24 AM from point source releases at Cayo Icaco and Cayo Lobos.

Figure 4.18: Visual comparison between computed particle positions and an aerial picture from Google Earth showing a suspended sediment plume.

Bibliography

Acevedo, R., Morelock, J., and Olivieri, R. A. (1989). Modification of coral reef zonation by terrigenous sediment stress. *Palaios*, 4:92–100.

Anselmi, C., Canals, M., Morell, J., Gonzalez, J., Capella, J., and Mercado, A. (2012). Development of an operational nearshore wave forecast system for Puerto Rico and the U.S. Virgin Islands. *Journal of Coastal Research*, 28(5):1049–1056.

Buttolph, A. M. B., Reed, C. W., Kraus, N. C., Ono, N., Larson, M., Camenen, B., Hanson, H., Wamsley, T., and Zundel, A. K. (2006). Two-dimensional depth-averaged circulation model CMS-M2D: Version 3.0, Report 2: Sediment transport and morphology change. Technical Report ERDC/CHL TR-06-09, U.S. Army Engineer Research and Development Center, Vicksburg, MS.

Canals, M. (2014). On the spatial distribution of the wave energy resource in Puerto Rico and the United States Virgin Islands. *submitted to the Journal of Renewable Energy*.

Canals, M., Morell, J., Corredor, J., and Leonardi, S. (2012). Expanding the Caribbean Coastal Ocean Observing System into the nearshore region. In *Oceans, 2012*, pages 1–4.

Coastal Processes Research Group (2007). State of Sebastian Inlet report: An assessment of inlet morphologic processes, historical shoreline changes, and regional sediment budget. Technical Report Technical Report 2007-1, Sebastian Inlet Tax District.

Dietrich, J., Trahan, C., Howard, M., Fleming, J., Weaver, R., Tanaka, S., Yu, L., Jr., R. L., Dawson, C., Westerink, J., Wells, G., Lu, A., Vega, K., Kubach, A., Dresback, K., Kolar, R., Kaiser, C., and Twilley, R. (2012). Surface trajectories of oil transport along the northern coastline of the gulf of mexico. *Continental Shelf Research*, 41(0):17 – 47.

King, D. B., Lackey, T. C., Gailani, J. Z., and Shafer, D. J. (2012). Fate of suspended dredge material at Apra Harbor, Guam: Particle tracking around coral reefs. In *Proceedings of the 12th International Coral Reef Symposium*, Cairns, Australia.

Lin, L., Kraus, N. C., and Barcak, R. G. (2004). Modeling sediment transport at the mouth of the Colorado River, Texas. In *Proceedings 8th International Estuarine and Coastal Modeling Conference*, pages 988–1006. ASCE.

MacDonald, N. J., Davies, M. H., Zundel, A. K., Howlett, J. D., Demirbilek, Z., Gailani, J. Z., Lackey, T. C., and Smith, J. (2006). PTM: Particle Tracking Model Report 1: Model Theory, Implementation, and Example Applications. Technical Report ERDC/CHL TR-06-20, U.S. Army Engineer Research and Development Center, Vicksburg, MS.

Sanchez, A. (2008). Interactions between wetlands and tidal inlets. Technical Report ERDC/CHL CHETN-IV-72, U.S. Army Engineer Research and Development Center, Vicksburg, MS.

Taylor, L. A., Eakins, B. W., Warnken, R. R., Carignan, K. S., Sharman, G. F., and Sloss, P. W. (2006). Digital elevation models for San Juan and Mayagüez, Puerto Rico: Procedures, data sources and analysis. Technical report, NOAA National Geophysical Data Center, Boulder, CO.

Wu, W., Sánchez, A., and Zhang, M. (2010). An implicit 2D depth-averaged finite-volume model of flow and sediment transport in coastal waters. In *ICCE Conference*, Shanghai, China.

Zarillo, G. A., Zarillo, K. A., and Finnegan, C. R. (2009). Physical characterization of nearshore and offshore borrow sites on the inner continental shelf of Northeast and West Florida. *Journal of Coastal Research*, 56:1095–1099.